A Power Efficient Pattern Synthesis Algorithm for Travelling Wave Microstrip Patch Antenna Arrays: Application to Mobile Base Station Antennas

by

Cameron Alakija

B.A.Sc., Simon Fraser University, 1990

THESIS SUBMITTED IN PARTIAL FULFILLMENT OF

THE REQUIREMENT FOR THE DEGREE OF

MASTER OF APPLIED SCIENCE

in the

School of Engineering Science

SIMON FRASER UNIVERSITY

November 25, 1991

ISBN 0-315-78169-6

APPROVAL

Name: Cameron Alakija

Degree: Master of Applied Science

Title of Thesis: A Power Efficient Pattern Synthesis Algorithm for Travelling Wave Microstrip Patch Antenna Arrays: Applications to Mobile Base Station Antennas

Examining Committee:

Chair: John Jones
Graduate Chairman and Professor
School of Engineering Science

Senior Supervisor: Shawn Stapleton
Assistant Professor
School of Engineering Science

Supervisor: Steve Hardy
Professor
School of Engineering Science

Examiner: John S. Bird
Associate Professor
School of Engineering Science

Date Approved: November 26, 91

PARTIAL COPYRIGHT LICENSE

I hereby grant to Simon Fraser University the right to lend my thesis, project or extended essay (the title of which is shown below) to users of the Simon Fraser University Library, and to make partial or single copies only for such users or in response to a request from the library of any other university, or other educational institution, on its own behalf or for one of its users. I further agree that permission for multiple copying of this work for scholarly purposes may be granted by me or the Dean of Graduate Studies. It is understood that copying or publication of this work for financial gain shall not be allowed without my written permission.

Title of Thesis/Project/Extended Essay

"A Power Efficient Pattern Synthesis Algorithm for Travelling Wave Microstrip Patch Antenna Arrays: Application to Mobile Base Station Antennas"

Author:

(signature)

Cameron ALAKIJA

(name)

November 27, 1991

(date)

ABSTRACT

A mobile communications base station, which utilizes a cylindrical array antenna, is presented. A scanning antenna pattern can be achieved by arranging a number of travelling wave patch antennas in a cylindrical array configuration. Using a switching matrix, different subsets of antenna elements, on the array, can be excited, thus producing a narrow steerable beam. Narrow scanning beams allow these base station antennas to retain both the high gain characteristic of directional antennas as well as the multidirectional characteristic of omnidirectional antennas. For a given transmit power such base stations can broadcast greater distances than omnidirectional base stations, while still being able to communicate with users in a 360° radius (at different time intervals). Another advantage of these base station antennas, over omnidirectional antennas, is that they can be placed closer together without interference. This form of frequency reuse means that a larger number of mobile users can be concentrated in a smaller area without increasing spectrum allocation.

Shaping the antenna pattern, in the elevation plane, can bring about certain advantages. Pattern shaping can help with tapering the antenna gain from the horizon down towards the earth, thereby increasing signal strengths to mobile units at larger distances from the base station. A pattern synthesis technique for travelling wave microstrip patch antennas is presented which takes into account both pattern shape as well as power efficiency. The algorithm, which uses an optimization routine, is suitable for synthesizing any desired antenna pattern. Simulated and measured results indicate good performance of this algorithm. A travelling wave antenna was designed, using this algorithm, which has 16 patches and a power efficiency of 73%.

ACKNOWLEDGEMENTS

I would like to acknowledge my supervisor, Dr. Shawn Stapleton, for directing this work and coming up with many useful suggestions. Mr Sirooj Rambaran who supplied the needed antennas for the test range as well as many useful suggestions. Mr. Gurmail Singh Kandola who contributed significantly in the implementation of the antenna range. Also the members of the Microwave/RF group at SFU whose occasional help was much appreciated.

TABLE OF CONTENTS

1 INTRODUCTION 1

2 A MOBILE BASE STATION CYLINDRICAL ARRAY ANTENNA 5
2.1 System Description 5
2.2 Radiators 7
2.3 Circular Array Theory 10
2.4 H-Plane Calculated Patterns 14
2.5 Switching Matrix 18
2.6 Beam Forming Feed 21

3 MICROSTRIP PATCH TRAVELLING WAVE ANTENNA 22
3.1 Patch Antenna Theory: Transmission Line Model 24
3.1.1 End Effects 28
3.1.2 Insertion Phase 29
3.2 Non-Uniform Unevenly spaced Linear Array Theory 30
3.3 Travelling Wave Antenna Theory 30
3.3.1 T-Matrix Representation 31
3.3.2 Optimum Power Efficiency Condition 35
3.3.3 Phase Distribution 38
3.4 Optimization Algorithms 39
3.5 Optimization Technique 44
3.6 Description of Algorithms 45

4 ANTENNA RANGE DESIGN AND CHARACTERISTICS 49
4.1 Antenna Range Theory 50
4.2 Far-Field Condition Calculations 52
4.3 Antenna Range Block Diagrams 52
4.3.1 HP8510 Network Analyzer 54
4.3.2 Tripods and Pedestals 54
4.3.3 System Controller 54
4.4 System Software 55
4.4.1 Main Menu 55
4.5 Time Domain Gating Considerations 58
4.6 Range Site Selection Criterion 60
4.7 Range Specification and Verification 61

5 RESULTS AND DISCUSSION 70

6 CONCLUSIONS 82

7 REFERENCES 83

TABLE OF FIGURES

Figure 1.1 Digital communication system with scanning beam 2
Figure 1.2 Adaptable cells. 3
Figure 1.3 The need for vertical pattern shaping 4
Figure 2.1 Cylindrical array of patches. 6
Figure 2.2 Sub array element excitation. 6
Figure 2.3 Antenna system diagram. 7
Figure 2.4 Patch antenna orientation. 8
Figure 2.5 E and H plane space factors of a typical patch. 10
Figure 2.6 Circular array geometry. 11
Figure 2.7 Geometry for calculating phase distribution. 15
Figure 2.8 Patterns with different phase distributions. 16
Figure 2.9 Varying numbers of excited elements. 17
Figure 2.10 Antenna patterns versus array radius. 18
Figure 2.11 Switching matrix topology. 19
Figure 2.12 Antenna power distribution 20
Figure 3.1 Pattern obtained using Woodward's Method. 23
Figure 3.2 Current magnitude distribution. 23
Figure 3.3 Current phase distribution. 24
Figure 3.4 Transmission Line Model of a patch. 25
Figure 3.5 Radiation conductance curve. 26
Figure 3.6 Resonant length versus width. 29
Figure 3.7 Delta versus width. 30
Figure 3.8 Travelling wave patch array. 31
Figure 3.9 S-Parameter calculation. 32
Figure 3.10 Calculated optimum current distribution. 38
Figure 3.11 Design algorithm flowchart. 46
Figure 4.1 A general model of an antenna range. 50
Figure 4.2 Block diagram of the antenna range. 53
Figure 4.3 Explanation of dynamic gating. 57
Figure 4.4 Different path lengths in an array. 60
Figure 4.5 Antenna range site. 61
Figure 4.6 Measured pattern (E-Plane) (1GHz). 63
Figure 4.7 Pattern measured by AEL (E-Plane) (1GHz). 63
Figure 4.8 Measured pattern (E-Plane) (4GHz). 64
Figure 4.9 Pattern measured by AEL (E-Plane) (2GHz). 64
Figure 4.10 Measured pattern (H-Plane) (1GHz). 65
Figure 4.11 Pattern measured by AEL (H-Plane) (1GHz). 65
Figure 4.12 Measured pattern (H-Plane)(2GHz). 66
Figure 4.13 Pattern measured by AEL (H-Plane) (2GHz). 66
Figure 4.14 Pattern of S-Band horn (gating) (H-Plane). 68
Figure 4.15 Pattern of S-Band horn (no gating) (H-Plane). 68
Figure 4.16 Pattern of S-Band horn (gating) (E-Plane). 69
Figure 4.17 Pattern of S-Band horn (no gating)(E-Plane). 69
Figure 5.1 First design simulated radiation patterns. 71
Figure 5.2 First design current amplitude distribution. 71
Figure 5.3 First design current phase distribution. 72
Figure 5.4 First design circuit board layout. 73
Figure 5.5 First design measured radiation patterns. 74
Figure 5.6 First design measured S-parameters. 75

Figure 5.7 Second design simulated radiation patterns. 76
Figure 5.8 Second design current amplitude distribution. 77
Figure 5.9 Second design current phase distribution. 77
Figure 5.10 Second design circuit board layout. 78
Figure 5.11 Second design measured S-parameters. 79
Figure 5.12 Second design measured patterns. 80
Figure 5.13 Second design re-simulated patterns. 80

LIST OF TABLES

Table 4.2 Minimum distance values with D varying 52
Table 5.1 Parameters of first array design 75
Table 5.2 Parameters of second array design 81

1 INTRODUCTION

In recent years the need for adaptive antennas in mobile communication systems has been steadily growing. Antennas with narrow steerable beams have the advantages of high antenna gain while retaining the multidirectional capabilities of omnidirectional antennas. This means that transmitted power levels can be reduced without any degradation of received signal strength. This is a great advantage since using lower transmit power translates to longer battery life and simpler amplifier design. Since there has recently been much concern about the biological effects of radiation, reducing transmitted power is quite desirable.

In digital mobile networks, this type of antenna can be used to realize improved performance in throughput. Figure 1.1 shows a simplified mobile digital communication network in which a contention based acquisition method is used. Since the gain of this antenna is higher than that for an omnidirectional antenna, the mobile sites can be located further away. The beam scans rapidly until it locates a mobile user needing to transmit and then it locks on to that user so data transmission can occur. At this time, mobile stations transmitting from other directions are blocked, reducing network collisions. The beam then continues scanning looking for other users. So the main advantages realized in such a system are that the mobiles can be further from the base station and collisions are reduced.

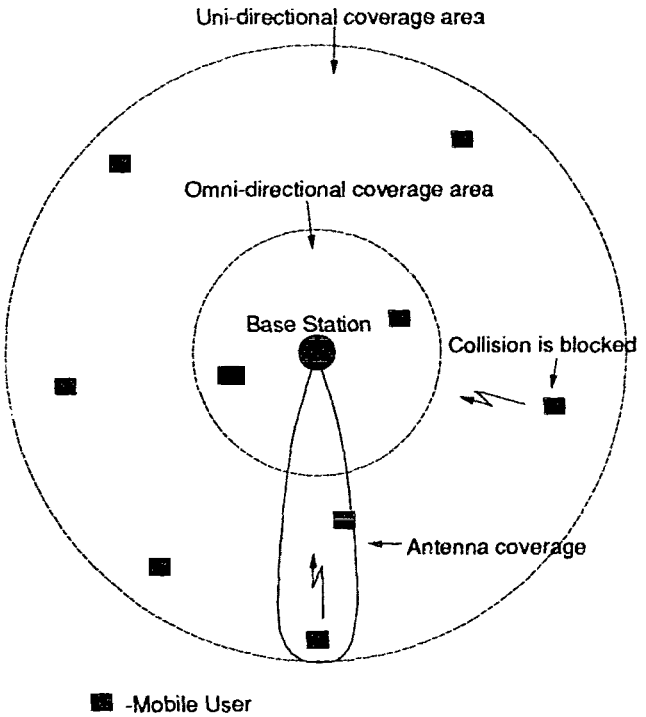

Figure 1.1 Digital communication system with scanning beam.

Another advantage associated with using steerable beam antennas is reduced interference. Due to the directionality of the antenna beam, there is less noise and interference power received at the base station. There is also lower generation of interference from the base station when it transmits. This means that base stations can be placed in closer proximity to one another. This form of frequency reuse means more users can be accommodated in a given area.

In cellular communication systems, the traffic load varies with time. Having adaptively shifting cells means that coverage can be increased in highly loaded city centers during daytime hours and then shifted outward during the evenings. Having a variable antenna beamwidth means cell size can also be changed dynamically. This would be convenient from a systems point of view since cells could be changed quickly and easily to match changing customer demand.

Another approach to frequency reuse is to sectorize a cell using fixed narrow beam antennas. Using this approach can also increase the number of users on the network. However, each sector requires a large space consuming antenna. When there is no mobile user in that sector the sector hardware is being wasted. Since antennas and locations to put them are expensive this waste is undesirable. So using an adaptive beam antenna allows sectors to be created, destroyed and re-sized as needed (Figure 1.2).

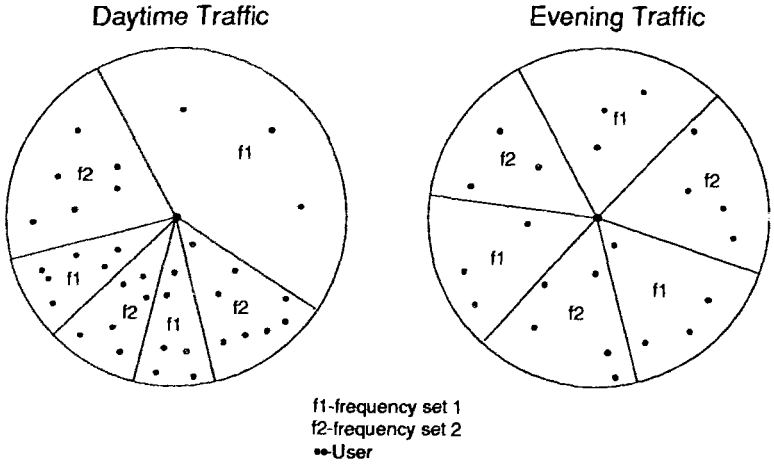

Figure 1.2 Adaptable cells.

Another beneficial design strategy involves producing an antenna which has a shaped beam in the vertical plane. Antennas, such as the dipole, have omnidirectional antenna patterns which waste power by radiating in directions where no users are present. By beam shaping in the vertical plane, (Figure 1.3), the wasted power, being radiated upward and into the ground, can be reduced. Interference into adjacent cells could also be reduced. The increased gain realized by producing antennas with shaped beams would also mean that lower power levels could be used to transmit further distances.

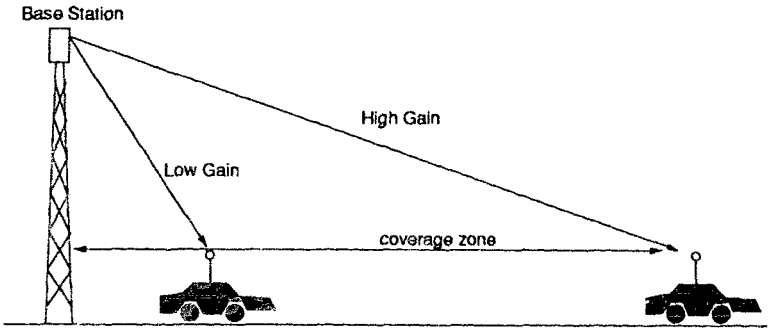

Figure 1.3 The need for vertical pattern shaping.

One of the difficulties in making patch antenna arrays cost and power efficient is in coming up with suitable feed networks for the array. Corporate feeds are both lossy, space consuming and complex for shaped patterns. For this reason the travelling wave antenna feed is ideally suited for microstrip patch arrays. This type of feed achieves the desired current distribution by varying the width and spacing of patches spaced along a microstrip feedline. One of the main design issues is then developing a microstrip patch antenna array which has a shaped beam pattern and is physically realizable. This is the topic that will be focused on in this thesis. Some systems level analysis on a scanning beam antenna system was also performed which will be described in section 2. Section 3 describes a technique to synthesize a pattern on a travelling wave patch antenna array. Section 4 describes the antenna test range used to measure the travelling wave patch antenna and section 5 contains the simulated and measured results.

2 A MOBILE BASE STATION CYLINDRICAL ARRAY ANTENNA

This section describes an antenna system which is capable of providing a beam which scans 360° in the horizontal plane. Simulations and analysis were done which show the performance that is attainable with such a system. Some of the key difficulties with this type of antenna, as well as some likely solutions, will be discussed.

2.1 System Description

As stated previously the antenna has to scan in a 360° radius. A good topology for such an antenna is a cylindrical array [1,2] (Figure 2.1). The beam direction is chosen by applying power to a subset of elements on the appropriate side of the array (Figure 2.2). For reasons which will be explained, a 32 element circular array in which 8 elements are active at once is a good design. This will allow for both a narrow enough beam width as well as efficient use of switches in the switching network.

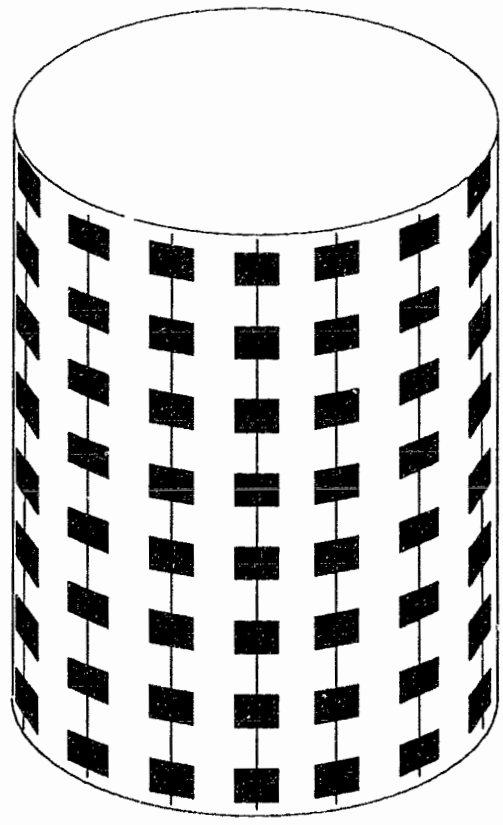

Figure 2.1 Cylindrical array of travelling wave patch antennas.

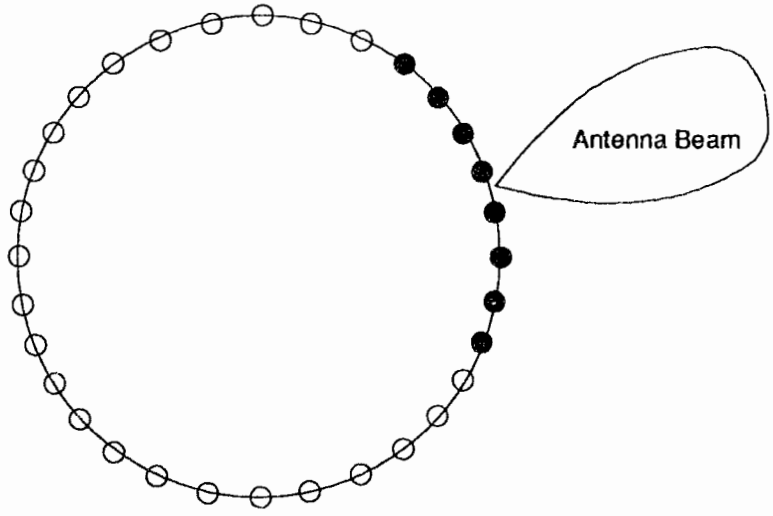

Figure 2.2 Sub element array excitation.

The proposed antenna system has three major subsystems: the radiating elements, the power and phase distribution network and the switching matrix. An optional subsystem is a matching network which may be needed for matching the feed network to the radiating elements. A block diagram showing major system components is shown in Figure 2.3.

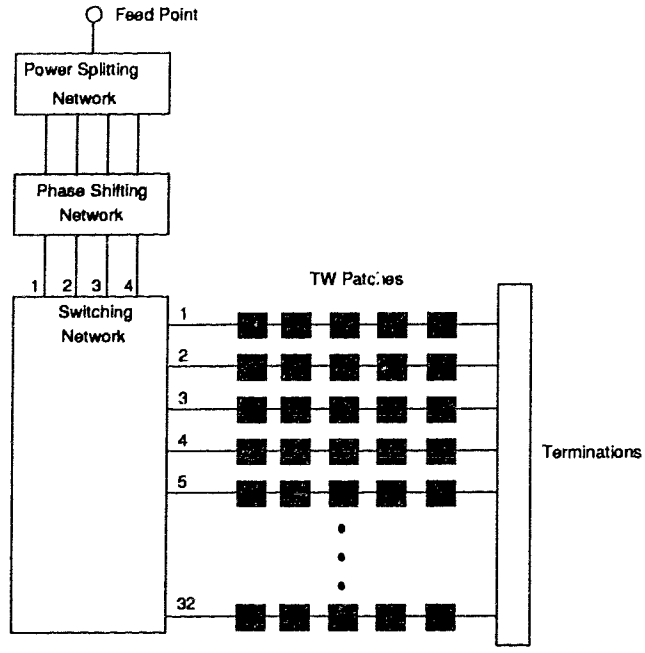

Figure 2.3 Antenna system diagram.

2.2 Radiators

The radiating elements chosen for the antenna array were microstrip patches. Patches are desirable due to their low cost and their extremely low profile. They are inexpensive to manufacture and due to the use of printed circuit techniques in their production, the design is highly repeatable. Since they are low profile, they also can be shaped conformally to cylindrical surfaces. They are ideal elements to use in cylindrical arrays since they have low back radiation. Due to their low profile they can be packaged in a format that is both mechanically sound as well

as practical.

There are some problems with patch antennas which make their use somewhat less attractive. Power efficiency of a patch antenna is usually quite low since the radiation resistance is typically in the order of a few hundred ohms. Since a patch antenna behaves much like a cavity resonator, it has a narrow VSWR-bandwidth, typically in the order of 2%. Wider VSWR-bandwidths, in the order of 7%, can be obtained using travelling wave antennas.

The radiation pattern of a rectangular microstrip patch is calculated using the transmission line model in [3]. The radiation pattern is like that of two slot antennas, separated by a distance l. The patch orientation used for the following derivation is shown in Figure 2.4.

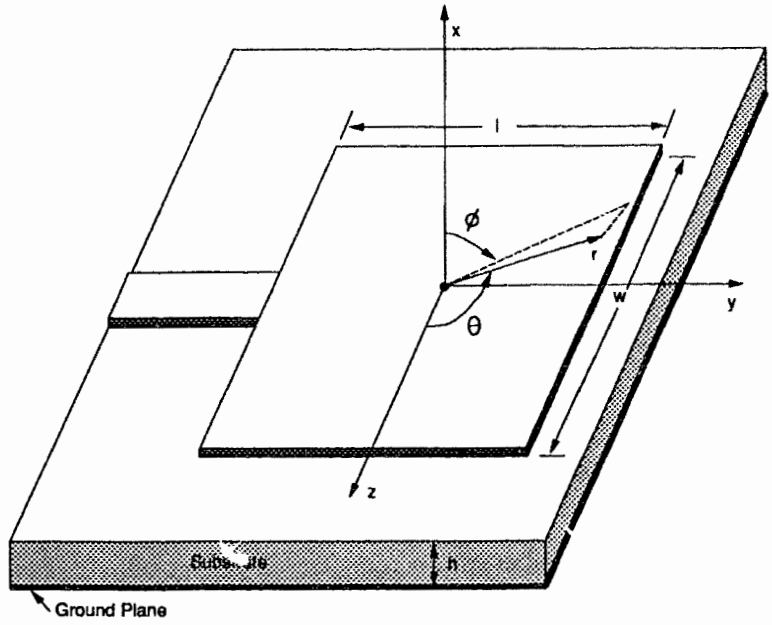

Figure 2.4 Patch antenna orientation.

It can be shown [3] that the far-field radiation from the patch is

$$E_r \approx E_\theta \approx 0 \tag{2-1a}$$

$$E_\phi(r,\theta,\phi) \approx -j\frac{hwkE_0e^{-jkr}}{\pi r}\left\{\sin\theta\left[\frac{\sin X}{X}\right]\left[\frac{\sin Z}{Z}\right]\right\}\cos\left(\frac{kl}{2}\sin\theta\sin\phi\right) \tag{2-1b}$$

for $0° \le \theta \le 180°$

and $-90° \le \phi \le 90°$

$E_\phi(r,\theta,\phi) = 0$ elsewhere

Where:

$$X = \frac{kh}{2}\sin\theta\cos\phi \tag{2-1c}$$

$$Z = \frac{kw}{2}\cos\theta \tag{2-1d}$$

E_0 is the electric field across the slot at the end of the patch and k is the free space propagation constant. The term $2\cos\left(\frac{kl}{2}\sin\theta\sin\phi\right)$ is the array factor of the two slot array. h is typically much smaller than a wavelength so (2-1b) reduces to

$$E_\phi(r,\theta,\phi) \approx -j2\frac{V_0e^{-jkr}}{\pi r}\sin\theta\left[\frac{\sin\left(\frac{kw}{2}\cos\theta\right)}{\cos\theta}\right]\cos\left(\frac{kl}{2}\sin\theta\sin\phi\right) \tag{2-2}$$

for $0° \le \theta \le 180°$

and $-90° \le \phi \le 90°$

$E_\phi(r,\theta,\phi) = 0$ elsewhere

Where $V_0 = h\,E_0$ is the voltage across the slot.

Since the r dependence of (2-2) is just an attenuation and a phase shift, the r dependence can be eliminated to get an equation which represents the normalized antenna pattern as a function of spatial angle. This is called the space factor of the patch antenna. The E and H plane patterns of a typical microstrip patch antenna are plotted on a dB scale in Figure 2.5.

$$SF(\theta,\phi) = \sin\theta \left[\frac{\sin\left(\frac{kw}{2}\cos\theta\right)}{\cos\theta} \right] \cos\left(\frac{kl}{2}\sin\theta\,\sin\phi\right) \tag{2-3}$$

for $0° \le \theta \le 180°$

and $-90° \le \phi \le 90°$

$E_\phi(r,\theta,\phi) = 0$ elsewhere

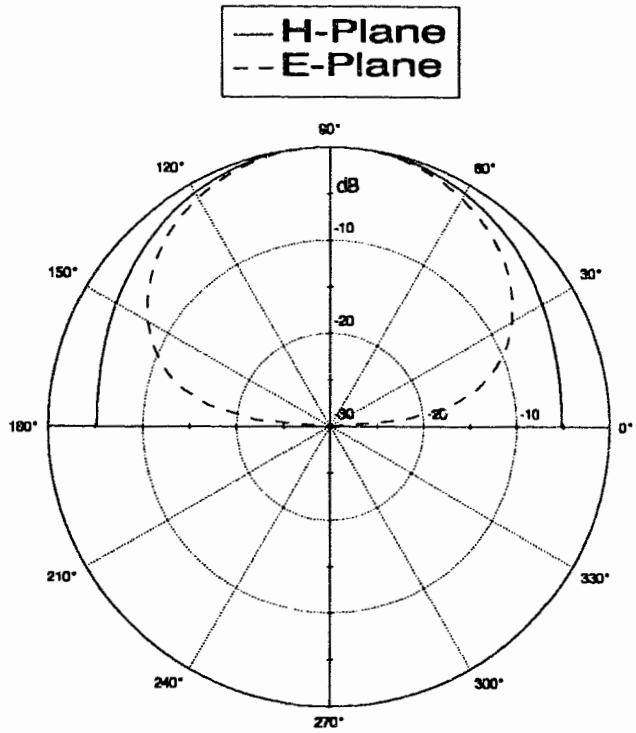

Figure 2.5 E and H plane patterns of a typical patch.

2.3 Circular Array Theory

A circular sector array is more difficult to calculate patterns for than a uniform linear array. Computer modelling simplifies this task somewhat. If the antenna is modeled by computer, the array parameters can be varied and changes in the pattern observed. Using analogies to linear arrays, an educated guess can be used to determine suitable initial parameters and then the

parameters can be optimized by hand or by program. In a uniform linear array with a broadside beam, element spacing of a half wavelength is typically used in order to obtain the best tradeoff between beamwidth and sidelobe levels [5]. In order to lower the sidelobes, the power should taper off towards the outside elements [5]. A circular sector array should follow roughly the same principles. In order to narrow the beam however, fixed phase shifters should be used to compensate for the curving of the array. Using variable phase shifters, instead of fixed phase shifters, allows for a certain amount of flexibility in the pattern beamwidth.

The geometry used to analyze a circular array [5] is shown in Figure 2.6.

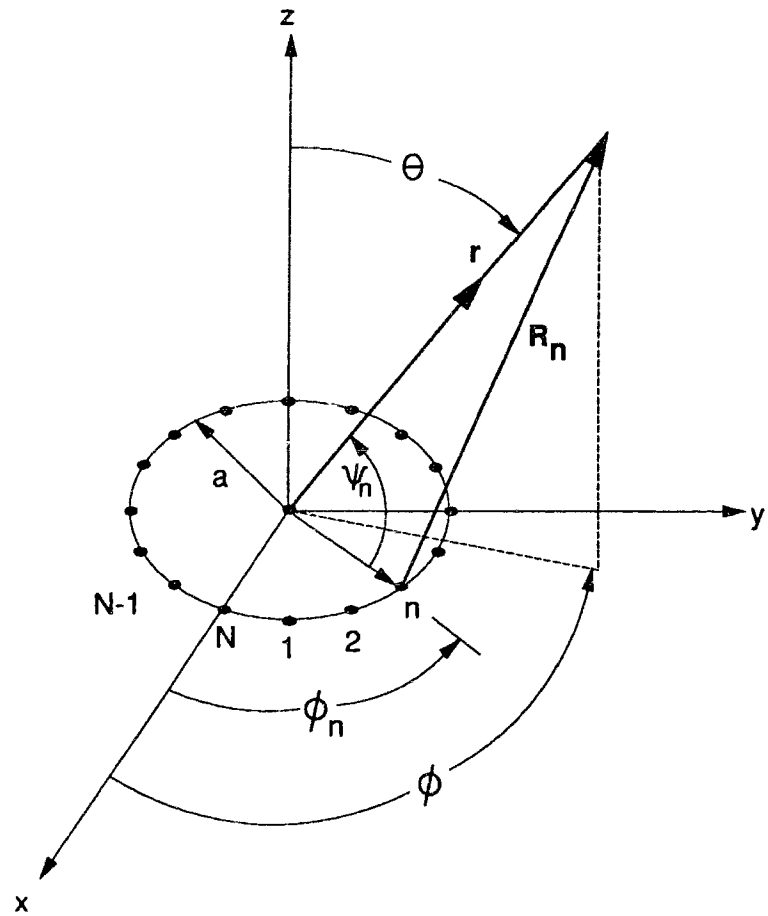

Figure 2.6 Circular array geometry.

Assuming far-field conditions and linear polarization the electric field from the array can be expressed by the following summation.

$$E_\phi(r,\theta,\phi) = \sum_{n=1}^{N} \frac{e^{-jkR_n}}{R_n} I_n SF_n(\theta,\xi_n) \tag{2-4}$$

$$\xi_n = \phi - \phi_n \tag{2-5}$$

$$\phi_n = 2\pi\left(\frac{n}{N}\right)$$

The term $SF_n(\theta,\xi)$ takes into account the magnitude variations of each patch as a function of angle. It can be computed using (2-3) with ϕ being replaced with ξ_n.

The term I_n is a complex number representing the square-root-magnitude and phase of the power to each patch. R_n can be computed using simple geometry.

$$R_n = [r^2 + a^2 - 2ar\cos(\psi_n)]^{0.5} \tag{2-6a}$$

Since $r \gg a$ this reduces to

$$R_n = r - a\cos\psi_n = r - a\sin(\theta)\cos(\xi_n) \tag{2-6b}$$

Assuming that for amplitude variations $R_n \approx r$, (2-4) reduces to

$$E_\phi(r,\theta,\phi) = \frac{e^{-jkr}}{r} \sum_{n=1}^{N} I_n SF_n(\theta,\xi_n) e^{jka\sin\theta\cos(\xi_n)} \tag{2-7}$$

Equation (2-7) assumes that the patch is oriented in the coordinate system shown in Figure 2.4 with the feedline running in the *y* direction. The travelling wave antennas must be oriented so the feedline runs in the *z* direction. A conversion formula to convert between coordinate systems is needed in order to adjust equation (2-7). The conversion formula should convert angles in

unprimed coordinates to angles in primed coordinates where the primed coordinates are obtained by rotating the unprimed coordinate system around the x-axis by +90°. In unprimed and primed coordinate systems the following equations are true.

$$x = r\sin\theta\cos\phi \tag{2-8}$$
$$y = r\sin\theta\sin\phi$$
$$z = r\cos\theta$$
$$x' = r\sin\theta'\cos\phi' \tag{2-9}$$
$$y' = r\sin\theta'\sin\phi'$$
$$z' = r\cos\theta'$$

If r=1 then

$$\sin\theta'\cos\phi' = x' = x = \sin(\theta)\cos(\phi) \tag{2-10}$$
$$\sin\theta'\sin\phi' = y' = z = \cos(\theta)$$
$$\cos\theta' = z' = -y = -\sin(\theta)\sin(\phi)$$
$$\theta' = \cos^{-1}(-\sin(\theta)\sin(\phi)) \tag{2-11a}$$
$$\phi' = \sin^{-1}\left(\frac{\cos\theta}{\sin\theta'}\right) \tag{2-11b}$$

In order to compute the patch magnitude variations in the unprimed coordinate system the primed coordinates using (2-11) must be calculated and used in (2-3). Equation (2-3) then becomes

$$SF'(\theta,\phi) = \sin\theta' \left[\frac{\sin\left(\frac{kw}{2}\cos\theta'\right)}{\cos\theta'} \right] \cos\left(\frac{kl}{2}\sin\theta'\sin\phi'\right) \tag{2-12}$$

where

$$\theta' = \cos^{-1}(-\sin(\theta)\sin(\phi))$$

and

$$\phi' = \sin^{-1}\left(\frac{\cos\theta}{\sin\theta'}\right)$$

The electric field vector is now vertically polarized so (2-7) is modified accordingly.

$$E_\theta(r,\theta,\phi) = \frac{e^{-jkr}}{r} \sum_{n=1}^{N} I_n SF'_n(\theta,\phi-\phi_n) e^{jka\sin\theta\cos(\phi-\phi_n)} \tag{2-13}$$

2.4 H-Plane Calculated Patterns

The cylindrical shape of this antenna increases the difficulty in analyzing the far field radiation pattern analytically. To compensate for this difficulty, a program was written which plots the radiation pattern of a cylindrical array of patches with arbitrary element excitation. Selection of appropriate array parameters can be accomplished by relating the theory used for periodic linear arrays to the cylindrical array. The main parameters to vary are the array radius, the number of elements, and the magnitude and phase of the power radiated by the elements.

The phase of the current distribution is chosen to try and correct for the curvature of the cylinder. Figure 2.7 shows the geometries involved in calculating the phase distribution.

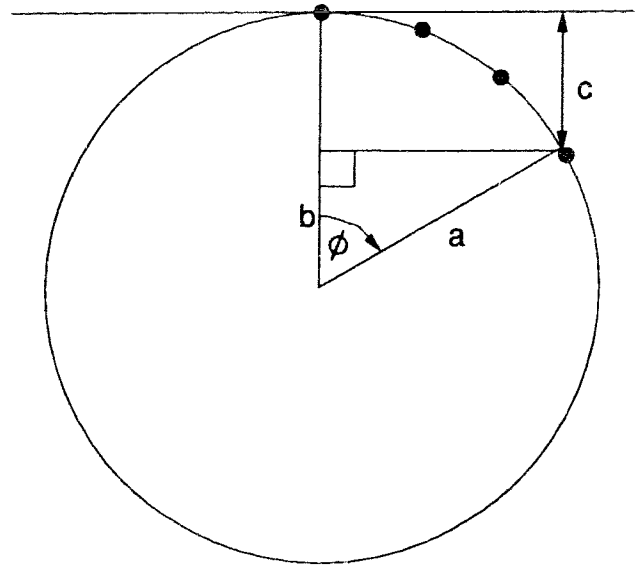

Figure 2.7 Geometry for calculating phase distribution.

Using simple geometry

$$c = a - a\cos\phi_n \tag{2-14}$$

Any phase shift which is constant to all elements can be deleted with no change to the pattern. Therefore, the phase distribution should be

$$\zeta = -ka\cos\phi_n \tag{2-15}$$

If (2-15) is included in (2-13) then (2-13) can be rewritten as

$$E_\theta(r,\theta,\phi) = \frac{e^{-jkr}}{r}\sum_{n=1}^{N} I_n SF'_n(\theta,\phi-\phi_n)e^{jka(\sin\theta\cos(\phi-\phi_n)-\cos\phi_n)} \tag{2-16}$$

A cosine amplitude distribution along the array surface was chosen in order to achieve a good tradeoff between beamwidth and sidelobe level. The chosen current distribution was found to give quite reasonable antenna patterns. This current distribution can however, be varied to cater to other pattern shapes. By altering the phase distribution, wider pattern beamwidths can be

obtained. This characteristic can be used to add another dimension of flexibility to the antenna in terms of variable sector size. Figure 2.8 shows different patterns obtained by varying the phase distribution. The patterns can be fine-tuned using optimization techniques.

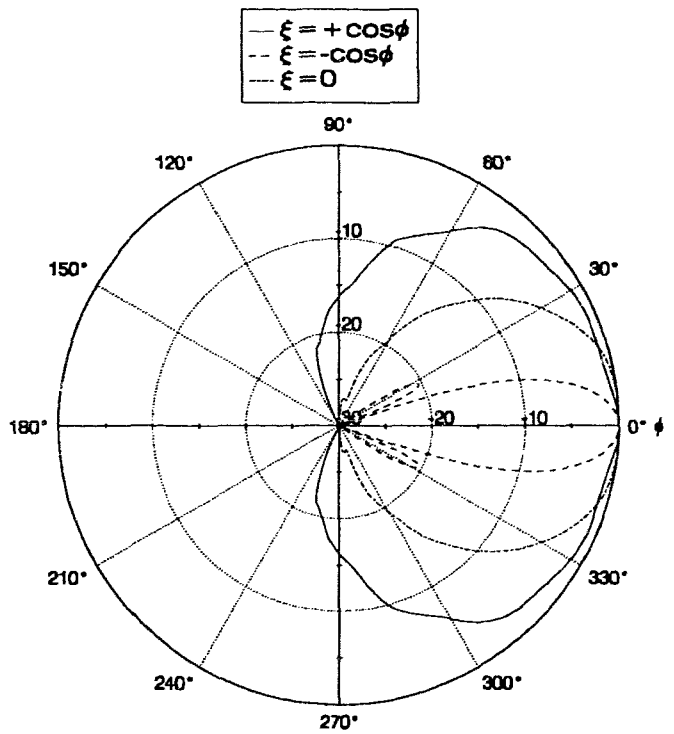

Figure 2.8 Simulated cylindrical array patterns with different phase distributions.

The number of elements needed for the array is mainly determined by the desired beamwidth and the scanning step size. The number of elements may also be adjusted to allow for switching matrix optimization. Due to the directional nature of the patch elements it is not useful to use elements that are more than 90 degrees from boresight. Otherwise, back lobes may increase considerably which will interfere with adjacent cells. It was found that a 32 element cylindrical array in which 8 elements are excited at a time will achieve a 12 degree scanning step size and a 20 degree beamwidth. Calculations show that a narrower beam can be obtained by increasing the number of elements which are excited in the array (Figure 2.9).

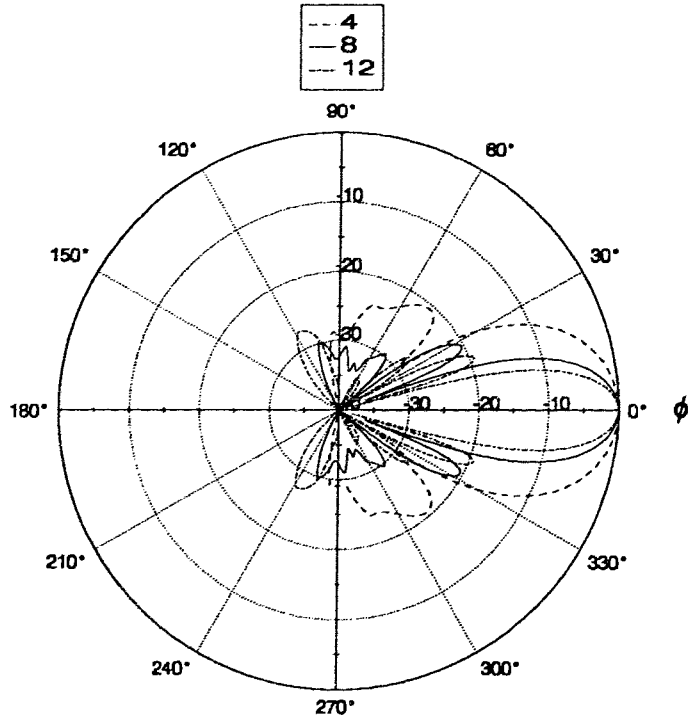

Figure 2.9 Patterns of a 32 element array with varying number of excited elements.

In linear arrays, the optimum spacing for maximum directivity and no grating lobes is $\lambda/2$ [5]. For a cylindrical array a similar analogy can be made. If the problem is looked at geometrically, a circular-sector array in which the sector angle is small can be approximated as a linear array. So if the elements are spaced a distance of $\lambda/2$ then the cylinder radius, a, must be chosen so that

$$\frac{2\pi a}{N} = \frac{\lambda}{2} \tag{2-17}$$

$$a = \frac{\lambda}{2\phi_n} \tag{2-18}$$

Calculations show that this radius is indeed close to the optimum value. Figure 2.10 shows the antenna pattern for circular arrays with varying values of radius. For an 800 MHz antenna,

(2-18) gives a radius value of 0.95. The figure also shows that by making the radius slightly larger, the beamwidth becomes narrower at the cost of higher side lobes. Making the radius smaller reduces side lobe levels at the cost of a wider beamwidth.

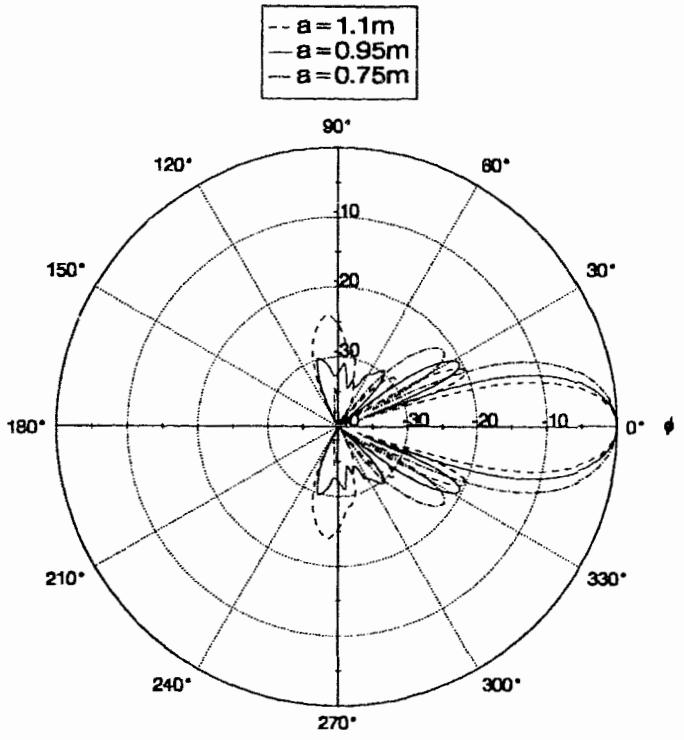

Figure 2.10 Antenna patterns versus array radius.

2.5 Switching Matrix

In order to facilitate the selection of different sub arrays it is necessary to use some kind of switching network. This allows one beam forming feed to distribute power to all sub-arrays. The switches used have to have the ability to handle a substantial level of power and should be as power efficient as possible. Due to the large power requirements as well as the fast switching

speeds of the antenna, PIN diode switches are the obvious choice. Diode switches with insertion losses of less than 1dB and isolation of 40 to 60 dB are possible to build. Most commercially available switches offer maximum power handling of 1 Watt.

A good topology for the switching network is shown in Figure 2.11. The switching network in Figure 2.11 forms a single antenna beam, on the 32 element array, by exciting 8 sequential array elements (Figure 2.12). There are four different power sources which are produced by the beam forming feed network (P1,P2,P3 and P4). Each of these power sources can be routed to two radiating elements at once. Since the current distribution is symmetrical, a single power source will be common to two elements. Due to the power loss in the switches, it is desirable to limit the number of switches the input signal has to pass through. Care must also be taken so that the switching network does not modify the current distribution in any way.

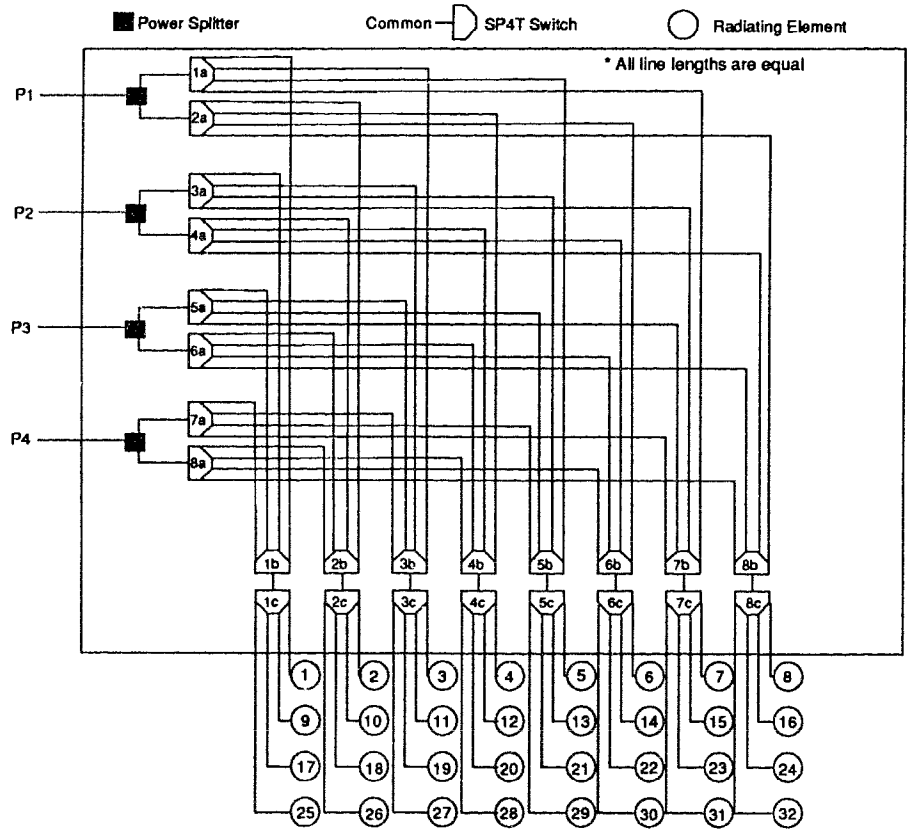

Figure 2.11 Switching matrix topology.

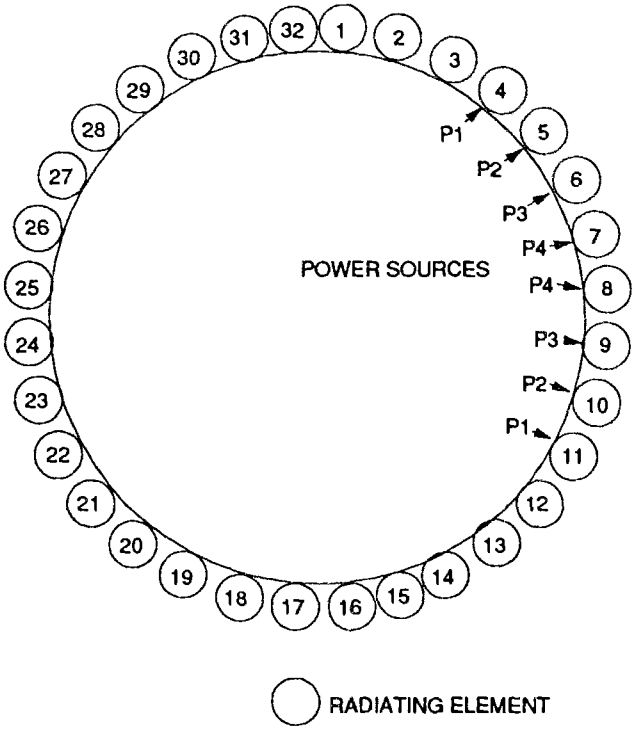

Figure 2.12 Antenna power distribution.

Pin diode switches usually have two ratings for power. The amount of continuous power they can handle and the amount of power they can handle during switching. When a pin diode is being switched its impedance is being changed from high impedance to low impedance. During this transition the impedance passes very close to the 50Ω standard impedance. So during this time the diode is dissipating the power passing through the switch. At the high impedance and low impedance points it is simply reflecting the majority of this power. Switching while RF power is passing through the switch is known as hot switching. Typically switches that are used for hot switching require a higher power rating than a switch used for cold switching. To get around this problem a single very high power switch can be used to disconnect the RF power from the switching matrix while it is switching.

2.6 Beam Forming Feed

The beam forming feed network splits the power from a single source into multiple sources with relative amplitudes and phases. By choosing appropriate amplitude and phase distribution a beam with both a narrow beamwidth and low sidelobes can be formed. The phase shifting in the network compensates for the circular shape of the array and maps the elements onto a linear wave front. The power distribution network is used to obtain a triangular or $\cos^n$ power distribution to the radiators. The phase shifters can be implemented using lengths of transmission line and the power distribution network will likely utilize some kind of microstrip corporate feed network [6].

Many types of microstrip power dividers are available including Wilkinson splitters [4] and coupled line sections[4]. Corporate feeds can also be constructed using tapered microstrip lines [4]. The type of feed that is most suited to uneven power distributions is the Wilkinson splitter. Using this type of feed network the amount of power loss can be kept to a minimum. Care must be taken when designing the power splitting network to ensure that any differences in phase between output ports is accounted for.

The phase shift network is perhaps one of the easiest subsystems to design. If a fixed phase shifter is required, a length of transmission line will be sufficient. In order to produce a variable phase shifter there are a number of methods available. One of the simplest methods is to use a PIN diode switch to switch in different lengths of transmission line into the circuit. The switches should be designed quite carefully to prevent unnecessary power loss.

3 MICROSTRIP PATCH TRAVELLING WAVE ANTENNA

In this chapter a pattern synthesis algorithm for travelling wave patch antennas will be discussed. For this type of antenna traditional beam synthesis techniques, such as the Fourier transform method [5], are not suitable since they lead to antennas with very low power efficiencies [7]. Using optimization techniques it is possible to obtain both the desired pattern and a current distribution that is power efficient and physically realizable.

Most classical array design algorithms are concerned with the synthesis of symmetrical, narrow beam patterns [5]. Classical current distributions [5] such as uniform, triangular, cosine and Taylor can be used to produce narrow, symmetrical beams with specified sidelobe levels. Adjusting the phase gradients along these arrays will squint the main beam angle from boresight. If the designer needs a simple symmetrical beam pattern then one of the above current distributions will be sufficient. However, these classical current distributions may lead to travelling wave antenna designs which are not as power efficient as they could be.

When arbitrarily shaped patterns have to be synthesized, the typical methods used are the Fourier Transform Method or Woodward's Method [5]. Figures 3.1, 3.2, and 3.3 show patterns and the resulting current distributions obtained using Woodward's Method. These methods usually lead to symmetrical current amplitude distributions which are highly peaked in the middle. The phase distributions are typically asymmetrical functions. Two problems arise when trying to implement these current distributions on a travelling wave patch array. Firstly, the peaked current distribution leads to power inefficiencies, in the antenna, resulting in reduced gain. Secondly, the Fourier Transform and Woodwards methods both assume that the array element spacing is uniform. Since the phase distribution, on a travelling wave antenna, is obtained by varying the spacing between the elements, the elements on a travelling wave array are not necessarily uni-

formly spaced. This means the solutions given by these methods are only approximate.

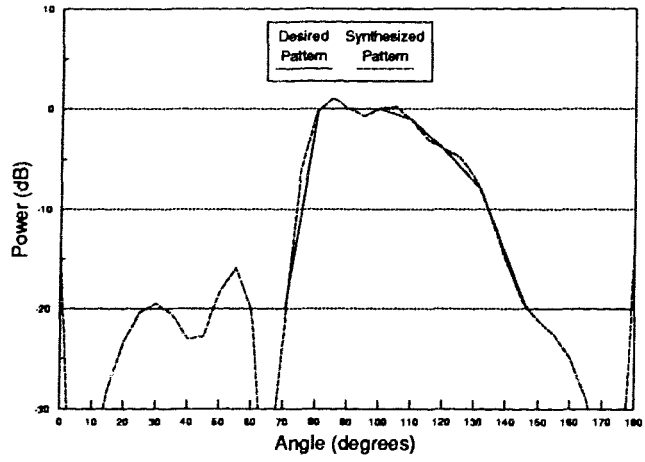

Figure 3.1 Pattern obtained using Woodward's Method.

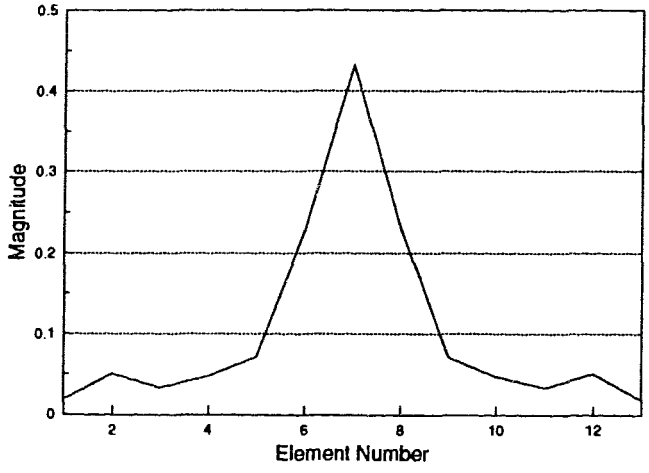

Figure 3.2 Current magnitude distribution using Woodward's Method.

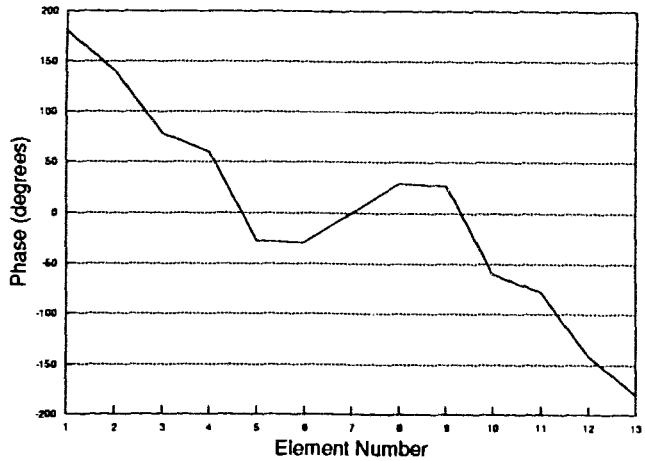

Figure 3.3 Current phase distribution using Woodward's Method

Other types of antenna synthesis algorithms use optimization techniques to synthesize arbitrary pattern shapes [5]. The task then is coming up with a suitable error function to minimize. In some optimizations the initial conditions may play a role in the final solution obtained. With complex multivariable functions, a number of local minima may be present causing optimization to be difficult. Therefore, experimenting with different optimization techniques may lead to faster and improved solutions.

3.1 Patch Antenna Theory: Transmission Line Model

There are a number of different models used for analyzing microstrip patches including the transmission line model [3] and the cavity model [6,8]. The cavity model has been recognized as a more complete and generalized model than the transmission line model. However, the transmission line model is more suitable for travelling wave antennas since each element can be represented as a two port T-matrix. The Transmission line model is also more computationally efficient than the cavity model so it is suitable for use in an optimization routine. Therefore, the discussion will be limited to the transmission line model.

The transmission line model was first described by Derneryd [3] in which a rectangular micro-strip patch was modeled as two slot radiators connected by a low impedance transmission line (Figure 3.4).

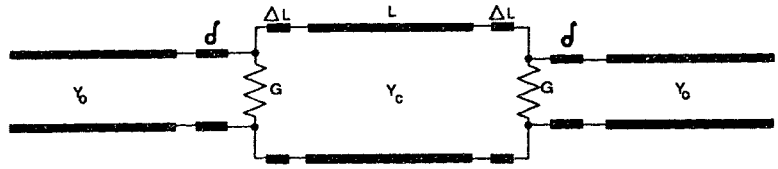

Figure 3.4 Transmission Line Model of a patch.

The radiation self conductance of each slot is computed using equation (3-1).

$$G_s = \frac{2P_{rad}}{|V_0|^2} \tag{3-1}$$

Where V_0 is the slot voltage and P_{rad} is the radiated power which is computed by integrating the Poynting vector over the hemisphere of radiation. The Poynting vector [5] is given by

$$\mathbf{W} = \frac{1}{2}(\mathbf{E} \times \mathbf{H}^*) = \frac{1}{2}(E_\phi H_\theta)\hat{a}_r \tag{3-2}$$

$$H_\theta = \eta E_\phi \qquad \text{so}$$

$$\mathbf{W} = \frac{1}{2}\eta |E_\phi|^2$$

E_ϕ is obtained by computing the radiation pattern from a single slot in the patch. E_ϕ is represented by equation (2-2) without the array factor $2\cos\left(\frac{kl}{2}\sin\theta\sin\phi\right)$ included.

$$E_\phi(r,\theta,\phi) \approx -j\frac{V_0 e^{-jkr}}{\pi r} \sin\theta \left[\frac{\sin\left(\frac{kw}{2}\cos\theta\right)}{\cos\theta}\right] \tag{3-3}$$

Therefore the Poynting vector is

$$W = \frac{1}{2}\eta \frac{|V_0|^2}{\pi^2 r^2} \frac{\sin^2\theta}{\cos^2\theta} \sin^2\left(\frac{kw}{2}\cos\theta\right) \tag{3-4}$$

and the radiated power is

$$P_{rad} = \int_{-\pi/2}^{\pi/2} \int_{0}^{\pi} W r^2 \sin\theta d\theta d\phi \tag{3-5}$$

$$= \pi \int_{0}^{\pi} W r^2 \sin\theta d\theta$$

Substituting (3-5) into (3-1) gives

$$G_s = \frac{\eta}{\pi} \int_{0}^{\pi} \frac{\sin^2\left(\frac{kw}{2}\cos\theta\right)}{\cos^2\theta} \sin^3\theta d\theta \tag{3-6a}$$

The above integral has to be solved numerically for different values of patch width. A typical curve is shown in Figure 3.5. The maximum radiation conductance obtainable is controlled by the maximum usable patch width. The width of the patch must be kept below about $1.2l$ otherwise different modes will develop in the patch leading to different patch behavior.

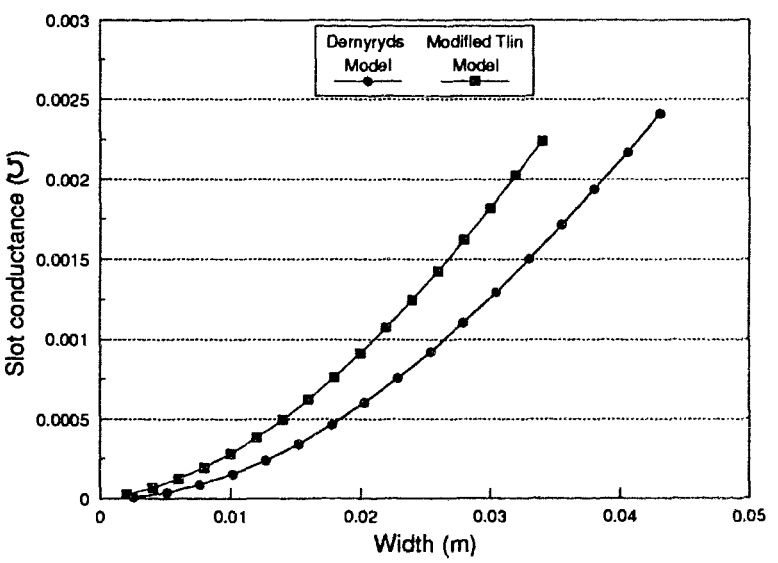

Figure 3.5 Radiation conductance curve (f=3.5 GHz. l=0.0272m).

The radiation conductance model developed above has some short comings in that it doesn't include the mutual coupling between the two ends of the patch. Another short coming in the model is that the width used is the physical patch width and not the effective patch width. The effective patch width includes effects such as fringing fields at the edges of the patch. A more accurate curve, for the radiation conductance, can be obtained by including mutual coupling and fringing effects into the calculation. This modified radiation conductance calculation comes from the so called modified transmission line model [4].

Reference [4] gives a derivation for the mutual conductance of two slots.

$$G_m = G_s\left\{J_0(kl) + \frac{(kh)^2}{24-(kh)^2}J_2(kl)\right\} \tag{3-6b}$$

The overall radiation conductance is then computed as

$$G = G_s + G_m \tag{3-6c}$$

Reference [4] also gives an expression for the effective patch width which should be used in place of w in equation (3-6a). This effective patch width is a direct result of fringing at the edges of the patch.

$$w_{eff} = 2\pi h / \ln\{hF/w' + \sqrt{1+(2h/w')^2}\} \tag{3-7a}$$

where

$$F = 6 + (2\pi - 6)\exp\left\{-\frac{4\pi^2}{3}\left(\frac{h}{w'}\right)^{3/4}\right\} \tag{3-7b}$$

$$w' = w + \frac{t}{\pi}\{1 + \ln(4/\sqrt{((t/h)^2 + (1/\pi)^2/(w/t+1.1)^2)}\} \tag{3-7c}$$

t is the thickness of the copper. A radiation conductance curve which takes mutual conductance and effective width into account is also shown in Figure 3.5.

3.1.1 End Effects

A capacitance or extra line length is included in the model to account for end effects [3]. The capacitance is equivalent to an extension of the transmission line by an amount ΔL. This is given approximately by the following empirical formula.

$$\Delta L = 0.412 \frac{\varepsilon_{eff} + 0.3}{\varepsilon_{eff} - 0.258} \frac{w/h + 0.262}{w/h + 0.813} \tag{3-8}$$

An open circuit transmission line which has a length less than $\lambda/4$ can be represented as an equivalent capacitance where

$$Z_{OC} = -jZ_0 \frac{\cos \beta d}{\sin \beta d} = -\frac{j}{\omega c} \tag{3-9}$$

For $d << \lambda$ $\cos \beta d \approx 1$ and $\sin \beta d \approx \beta d$ therefore

$$C \approx \frac{\beta d}{Z_0}$$

In practice it is easier to represent the end effect as an effective electrical length of the patch and reduce the physical length to compensate. The resonant length as a function of width, for the patches, was calculated using the Touchstone Microwave Simulation Program and is plotted in Figure 3.6. This variation of resonant length with width should be included in calculations. Another way to obtain this information is through direct measurement.

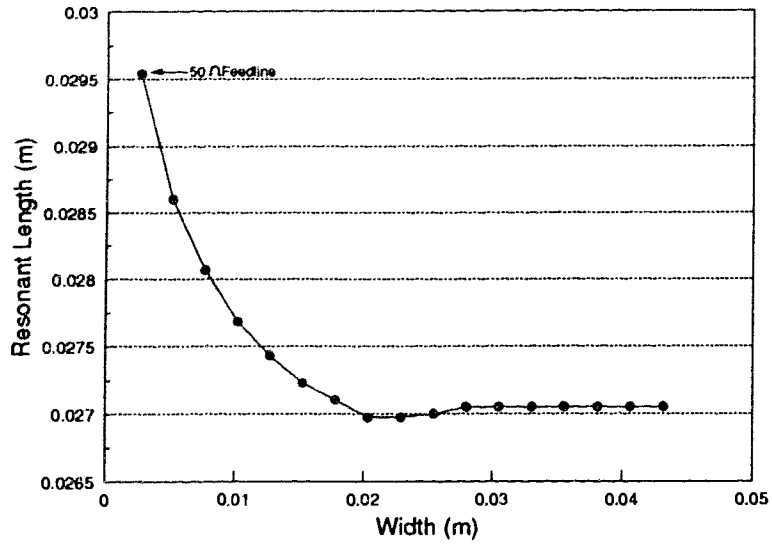

Figure 3.6 Resonant length versus width (f=3.5 GHz, er=2.48).

3.1.2 Insertion Phase

The insertion phase of a patch is the amount of phase shift obtained through the patch. Typically the amount of phase shift is close to 180° for narrow patches but increases for wider patches to values up to 210°. Since it was difficult to obtain a model for insertion phase, measured data from a paper [7] were used. It is important to account for this insertion phase in simulations as it affects the current distribution of the antenna. The insertion phase can be easily accounted for by adding an extra electrical length to the feedlines going out of each patch (the physical length should not change). The excess feedline length will be denoted as δ. A plot of δ as a function of width is shown in Figure 3.7.

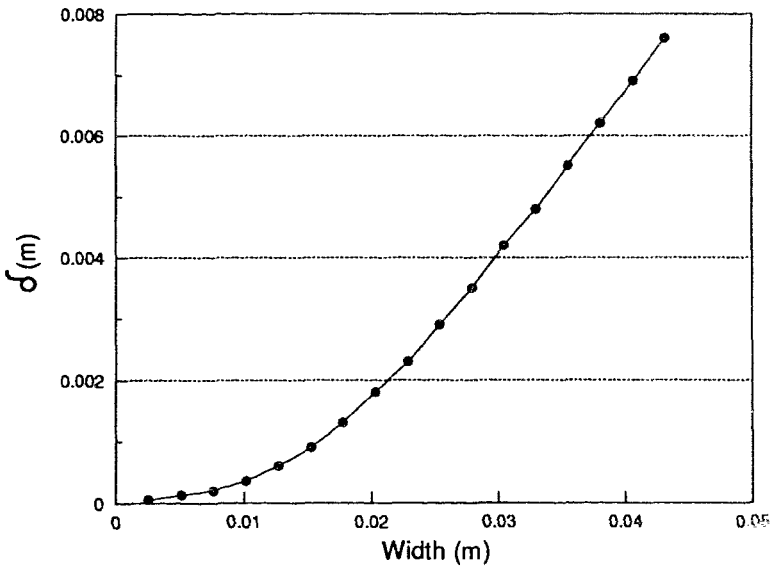

Figure 3.7 δ versus width (f=3.5GHz, er=2.48).

3.2 Non-Uniform Unevenly spaced Linear Array Theory

The array factor for an unevenly spaced array of non-uniform excitation is given by equation (3-10).

$$AF(\theta) = \sum_{n=1}^{N} a_n e^{jkd_n \cos\theta} \tag{3-10}$$

The array placement is along the z-axis, a_n is the complex excitation coefficient of the n^{th} array element and d_n is the distance to the n^{th} array element from the origin.

3.3 Travelling Wave Antenna Theory

A typical travelling wave patch antenna is shown in Figure 3.8. Power starts at the feed point and travels through the patches to the load. At the operating frequency the patches are resonant so their equivalent impedance is $2G$. As the power travels down the antenna towards the load,

power is radiated from the patches. The current distribution along the array is controlled by varying the position of the patches on the feedline and the patch widths. For an efficient antenna the majority of the input power would be radiated and a small fraction would be dissipated in the termination. Clearly the most efficient antennas would be ones in which the patches were quite wide and numerous. Increasing the feedline impedance allows for more efficient antennas. However, a matching network would be required somewhere to transform the feedline impedance to 50Ω. Increasing the feedline impedance higher than this is impractical since losses in the narrow feedline would start to dominate the efficiency calculation.

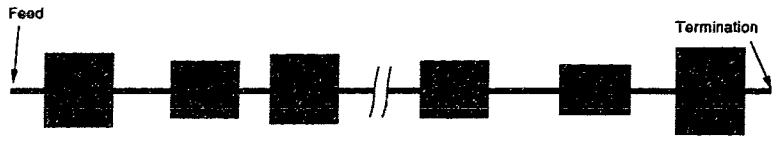

Figure 3.8 Travelling wave patch array.

3.3.1 T-Matrix Representation

A T-Matrix is a convenient way to relate the current distribution of an antenna to physical parameters such as feedline length and radiation conductance. Elements such as transmission lines and shunt conductances can be represented by the T-Matrix. When these elements are connected in series the T-matrices can be simply multiplied to compute the voltages at each node in the circuit.

The T-matrices for the transmission lines and the radiation conductances can be computed using techniques found in [9]. First the S-parameters for a lossy transmission line of arbitrary impedance will be computed. The circuit for computing the S-parameters is shown in Figure 3.9. The S parameters are referenced to Z_o.

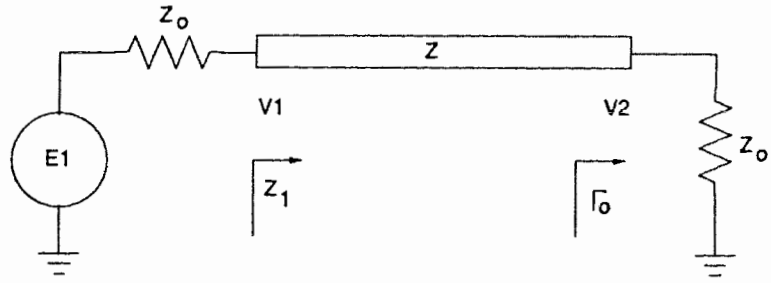

Figure 3.9 S-Parameter calculation.

From [9] it can be shown that

$$S_{11} = \frac{Z_1 - Z_o}{Z_1 + Z_o} \tag{3-11}$$

$$S_{21} = \frac{2V_2}{E_1} \tag{3-12}$$

Starting with S_{11} the equation for Z_1 is

$$Z_1 = Z\frac{Z_o \cosh(\gamma d) + jZ \sinh(\gamma d)}{Z \cosh(\gamma d) + jZ_o \sinh(\gamma d)} \tag{3-13}$$

Where:

$$\gamma = \alpha + j\beta = \sqrt{(R + j\omega L)(G + j\omega C)}$$

and

$$Z = \sqrt{\frac{R + j\omega L}{G + j\omega C}}$$

γ is the complex propagation constant with attenuation factor α given in nepers per meter and the propagation constant β given in radians per meter. R, L, G, C are the resistance, inductance , conductance and capacitance per unit length in the transmission line. Z is the complex transmission line impedance.

Plugging this into (3-11) and simplifying gives

$$S_{11} = \frac{j(Z^2 - Z_o^2)\sinh(\gamma d)}{2ZZ_o\cosh(\gamma d) + j(Z^2 + Z_o^2)\sinh(\gamma d)} \tag{3-14}$$

Solving for S_{21} is a little more complex. Using circuit theory the following is true.

$$V_1 = E_1 \frac{Z_1}{Z_o + Z_1} \tag{3-15}$$

The voltage along a transmission line can be computed using the following transmission line equation.

$$V_1 = \frac{V_2 e^{\gamma d}(1 + \Gamma_o e^{2\gamma d})}{(1 + \Gamma_o)} \tag{3-16}$$

Where:

$$\Gamma_o = \frac{Z_o - Z}{Z_o + Z}$$

Combining equation (3-15) and (3-16) allows S_{21} to be solved for.

$$S_{21} = 2\frac{V_2}{E_1} = \frac{2(1 + \Gamma_o)\frac{Z_1}{Z_o + Z_1}}{e^{\gamma d}(1 + \Gamma_o e^{2\gamma d})} \tag{3-17}$$

Simplifying, this equation becomes

$$S_{21} = \frac{2Z_o Z}{j(Z_o^2 + Z^2)\sinh(\gamma d) + 2Z_o Z\cosh(\gamma d)} \tag{3-18}$$

Due to the reciprocal nature of this device it is fairly clear that

$$S_{22} = S_{11} \qquad S_{12} = S_{21} \tag{3-19}$$

For the radiation conductance the S-parameters can be computed directly using equations from [9].

$$S_{11} = S_{22} = \frac{-Z_o g}{2 + Z_o g} \tag{3-20}$$

$$S_{21} = S_{12} = \frac{2}{2 + Z_o g} \tag{3-21}$$

The S-parameters can be converted to T-parameters using the following conversion formula [9].

$$\begin{bmatrix} T_{11} & T_{12} \\ T_{21} & T_{22} \end{bmatrix} = \begin{bmatrix} \frac{1}{S_{21}} & -\frac{S_{22}}{S_{21}} \\ \frac{S_{11}}{S_{21}} & S_{12} - \frac{S_{11} S_{22}}{S_{21}} \end{bmatrix} \tag{3-22}$$

A great deal of insight can be gained by looking at the preceding equations under various conditions. The parasitic resistance and conductance in the transmission lines introduce a phase shift in the line as well as an attenuation. If it is assumed that R and G are very small then the phase shift becomes negligible and only the attenuation needs to be included. The attenuation in a lossy line is an exponential function of distance. So the attenuation for a given length of line need only be computed and included in the simulation. For a transmission line with characteristic impedance Z_o, such as the feedline, the S-parameters become

$$\begin{bmatrix} S_{11} & S_{12} \\ S_{21} & S_{22} \end{bmatrix} = \begin{bmatrix} 0 & e^{-j\beta_f d} e^{-\alpha_f d} \\ e^{-j\beta_f d} e^{-\alpha_f d} & 0 \end{bmatrix} \tag{3-23}$$

The T-matrix is

$$\begin{bmatrix} T_{11} & T_{12} \\ T_{21} & T_{22} \end{bmatrix} = \begin{bmatrix} e^{j\beta_f d} e^{\alpha_f d} & 0 \\ 0 & e^{j\beta_f d} e^{\alpha_f d} \end{bmatrix} \tag{3-24}$$

The T-matrix for a lossy patch at resonance is

$$\begin{bmatrix} T_{11} & T_{12} \\ T_{21} & T_{22} \end{bmatrix} = \begin{bmatrix} -1e^{\alpha_p d} & 0 \\ 0 & -1e^{\alpha_p d} \end{bmatrix} \tag{3-25}$$

Equation (3-25) can be used to make calculations more efficient. If more accuracy is required or a frequency response has to be measured then the general equations (3-18) should be used. Equations (3-25) still provides some insight into what is actually happening in the antenna at resonance.

3.3.2 Optimum Power Efficiency Condition

In order to get good antenna power efficiency the antenna synthesis algorithm must try to achieve current distributions which use large values of patch widths. It will be shown that power efficient current distributions have a shape that depends on the maximum patch conductance and the feedline impedance. The maximum radiation conductance depends on the relative dielectric constant of the substrate used since the dielectric constant controls the length and width of the patch.

The S-parameters of a shunt conductance are

$$S_{11} = S_{22} = \frac{-Z_0 g}{2 + Z_0 g} \tag{3-26}$$

$$S_{12} = S_{21} = \frac{2}{2 + Z_0 g}$$

Since $1/g >> Z_0$ the term $Z_0 g << 1$ therefore

$$S_{11} \approx 0 \tag{3-27}$$

$$S_{12} = S_{21} = \frac{2}{2 + Z_0 g}$$

The power dissipated in the conductance is

$$P_{rad} = P_{in}(1 - S_{21}^2) = P_{in}\left[1 - \left(\frac{2}{2 + Z_0 g}\right)^2\right] \tag{3-28}$$

The power going out of the circuit is

$$P_{out} = P_{in} S_{21}^2 = P_{in}\left[\frac{2}{2 + Z_0 g}\right]^2 \tag{3-29}$$

If each element is set to the maximum radiation conductance possible then the power radiated at the n^{th} element is

$$P_n = P_{in}\left(\frac{2}{2 + Z_0 g_{\max}}\right)^{2(n-1)}\left[1 - \left(\frac{2}{2 + Z_0 g_{\max}}\right)^2\right] \tag{3-30}$$

Since the current distribution is the square-root of the power distribution, the current distribution should have the following form

$$a_n = a_{in}\left(\frac{2}{2 + Z_0 g_{\max}}\right)^{(n-1)}\left[1 - \left(\frac{2}{2 + Z_0 g_{\max}}\right)^2\right]^{\frac{1}{2}} \tag{3-31}$$

$$= a_{in} S_{21}^{(n-1)} C$$

So the optimum current distribution is in the form of a geometric series. The radiation loss can be expressed in an additive equation instead of a multiplicative equation if it is represented in dB. Other losses in the transmission line, due to leakage in the substrate and copper resistivity, can also be included in equation (3-31).

It will be emphasized here that the main assumption in developing equation (3-31) is that S_{11} and S_{22} are very small. If this is not the case then the power flow on the antenna feedline will start to have increasing reverse travelling components as well as forward ones. For the antenna in this thesis, which has a relative dielectric constant of 2.48, the maximum radiation conduction for the patch is G_{max}=0.00426. The corresponding S_{12} and S_{11} as calculated by (3-26) are

$$S_{12} = 0.904 \qquad (3\text{-}32)$$

$$S_{11} = -0.096$$

In order to verify equation (3-31) the current distribution of a uniform array of maximum width patches was computed using T-matrices. This current distribution was plotted in Figure 3.10 next to the current distribution computed by (3-31). The results were quite similar. Interesting to note is that the array with the 100Ω feedline has less power left near the end of the feedline. This shows that the antenna with the 100Ω feedline is more efficient than the one with the 50Ω feedline. In fact the 50Ω feed antenna has 5% of the power dissipating in the load while the antenna with the 100Ω feed has only 0.36% of the power dissipating in the load. Producing feedlines greater than 100Ω may be impractical since they are difficult to fabricate and are difficult to match to. Furthermore, the advantages gained by using high impedance lines will be lost due to the high series resistance of the narrow lines.

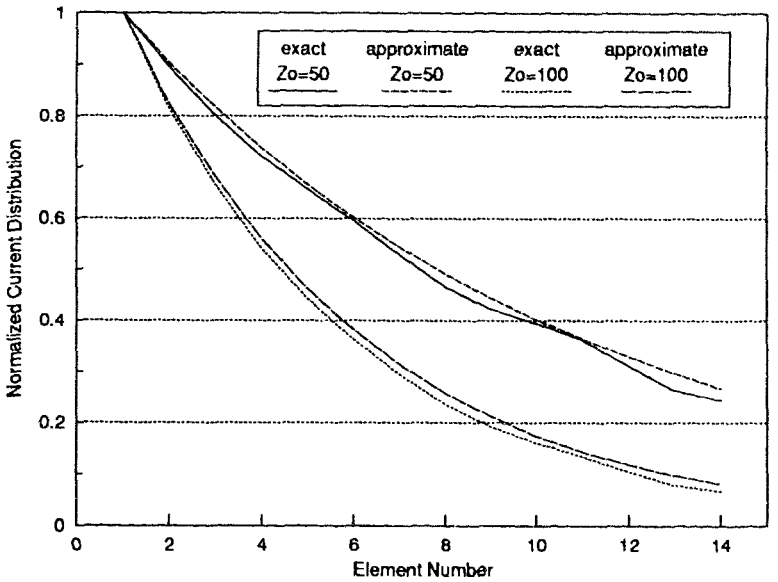

Figure 3.10 Calculated and actual optimum current distributions for power efficiency.

The optimization algorithm tries to force the magnitude of the antennas current distribution to be similar to the optimum current distribution. Doing this ensures that the antenna is physically realizable, in terms of patch widths, as well as power efficient.

3.3.3 Phase Distribution

The exact current distribution along a travelling wave patch antenna can be computed by using the T-matrix representation of the circuit. These T-matrix elements could conceivably be expanded from two-port devices to multi-port devices in order to include the effects of mutual coupling between elements. Since coupling is typically 20 dB below the radiated power, for patches in a travelling wave configuration, coupling will only affect the pattern sidelobes. So coupling is a second order effect and will be omitted from the calculations. For more stringent designs it may be necessary to compute the coupling and include it in the optimization.

The phase of the power to each element is controlled mainly by varying the electrical length of the feedlines. In fact, if the previous assumption of only a forward travelling wave is used, then the phase difference between two elements will be equal to the insertion phase of the patch plus the electrical length of the feedline between the elements. Unless, it is decided to have meandering feedlines the spacing of the antenna elements is also a function of the phase distribution to the elements.

This relation between phase distribution and patch spacing has several unfortunate drawbacks. Given a fixed magnitude and phase distribution to the elements, if the dielectric constant of the substrate is changed, the spacing of the elements will have to change. So the dielectric constant has to be chosen before design can begin. Another drawback of this relation between spacing and phase distribution is that rapidly varying phase distributions would require unusually long or short patch spacings. Since the average element spacing should be kept close to $\lambda/2$ this implies that the phase distribution of the elements is constrained by the spacing of the elements. One way to get around these problems is to use a meandering type of feedline so that the patch spacing can be fixed to $\lambda/2$. This may be difficult in antennas with low dielectric constants since the patch spacing is close and there isn't much room for a winding feedline. Furthermore a winding feedline may contribute undesired parasitic radiation.

3.4 Optimization Algorithms

As already shown in equation (3-10) the array factor for an unevenly spaced antenna is

$$AF(\theta) = \sum_{n=1}^{N} a_n e^{jkd_n \cos\theta} \tag{3-33}$$

The excitation coefficient for the elements has a magnitude and a phase where the phase is a function of the distance d_n, of the element from the feed point and of k_s, the propagation constant of the substrate.

$$AF(\theta) = \sum_{n=1}^{N} |a_n| e^{j\zeta_n} e^{jkd_n \cos\theta} \tag{3-34}$$

where

$\zeta_n \approx k_s d_n$

$$AF(\theta) = \sum_{n=1}^{N} |a_n| e^{jd_n(k\cos\theta + k_s)} \tag{3-35}$$

The variables in this equation are the magnitude excitation coefficients a_n and the distance d_n. The array factor at each angle is complex, however, for most situations the phase is not important. Many synthesis algorithms set this phase to zero, however, this practice sets an unnecessary constraint on the equation and reduces the number of solutions to the equation. Since the radiation pattern fit to the desired pattern must be good, while at the same time trying to obtain power efficiency, it would not be wise to impose such a constraint on the pattern phase distribution. If only the magnitude of the array factor is considered then equation (3-36) becomes increasingly difficult to solve using direct techniques.

$$|AF(\theta)| = \left| \sum_{n=1}^{N} |a_n| e^{jd_n(k\cos\theta + k_s)} \right| \tag{3-36}$$

In order to simplify calculations, a discrete number of angles should be chosen where (3-36) can be resolved. A sufficient number of points must be chosen to ensure pattern accuracy. With limited angles the problem now reduces to one of multiple equations with multiple unknowns.

Unfortunately, the equations are nonlinear and therefore can't be solved using standard matrix techniques. Furthermore, a method is also needed to include power efficiency into the calculation.

$$|AF(\theta_1)| = \left| \sum_{n=1}^{N} |a_n| e^{jd_n(k\cos\theta_1 + k_s)} \right| \tag{3-37}$$

$$|AF(\theta_2)| = \left| \sum_{n=1}^{N} |a_n| e^{jd_n(k\cos\theta_2 + k_s)} \right|$$

.

.

.

$$|AF(\theta_m)| = \left| \sum_{n=1}^{N} |a_n| e^{jd_n(k\cos\theta_m + k_s)} \right|$$

If initial conditions are chosen for element magnitude and spacing then an initial array factor can be computed. If the mean-squared error between the present array factor and the desired array factor is computed then the problem is reduced to one equation with multiple unknowns.

$$\varepsilon_{AF} = \frac{1}{m} \sqrt{\sum_{i=1}^{m} (|AF_{des}(\theta_i)| - |AF(\theta_i)|)^2} \tag{3-38}$$

Similarly the efficiency constraints on the excitation magnitudes can be represented in a similar equation. The current distribution needs to approximate the same shape as the optimum current distribution given in Figure 3.10. This is done by computing the mean-squared error between the calculated and desired current magnitudes.

$$\varepsilon_{pwr} = \frac{1}{N}\sqrt{\sum_{n=1}^{N}[|a_{des,n}| - |a'_n|]^2} \tag{3-39}$$

Where

$$a'_n = \frac{a_n}{a_{\max}}$$

a'_n is the normalized current distribution. Care must be taken to normalize the current distribution so that when it is compared to the optimum current distribution the values are the same order of magnitude. As stated previously in equation (3-31) the desired current distribution is geometric. The normalized expression is

$$a_{des,n} = S_{21}^{(n-1)} \tag{3-40}$$

The optimum design will be one in which equations (3-38) and (3-39) are both minimized (as close to zero as possible). To accomplish this dual minimization, a weighting function must be used to weight the error contributions from both pattern and current magnitude distribution. An optimization routine is then used to minimize this composite error function.

Some of the advantages of this technique are as follows. If the design parameters have to be constrained in any way then constraints can be included in the error function. By weighting these constraints in an appropriate way, using weighting factors or functions, variables can be constrained between certain limits. The difficulty arises in determining the weighting function or factor to be used. Certain optimization algorithms require functions to be continuous and have continuous derivatives. Therefore, care must be taken to use weighting functions which satisfy these requirements.

An exponential function is a useful function to constrain parameters (equation 3-41). If the value of the parameter is greater than the maximum value then the exponential function increases rapidly. If it is less than the maximum value then it drops off rapidly towards zero.

$$err(x) = S_1 e^{S_2(x-C)} \quad \text{can be used for the} \quad x \le C \quad \text{constraint} \tag{3-41}$$

and

$$err(x) = S_1 e^{S_2(C-x)} \quad \text{can be used for the} \quad x \ge C \quad \text{constraint}$$

The constant S_2 can be varied to control the sharpness of the function at the transition point and S_1 is a scaling constant. Caution should be taken not to make the transition too sharp otherwise the optimization algorithm may have difficulty converging.

Another advantage of this technique is that different sections of the pattern and/or current distribution can be weighted according to importance. For example if a designer needs to have a pattern null in a certain direction then he/she can weight this direction heavier than others to ensure this condition is met above others. Furthermore, since antenna patterns are usually specified on a decibel scale the least squares error between desired and calculated patterns can also be computed on a decibel scale. This is useful since pattern sidelobes which are represented on a linear scale will contribute only very small amounts to the least squares error leading, perhaps, to undesirably high sidelobes.

One of the major disadvantages to this technique is the amount of computation which has to be done to obtain a solution. In order to reduce the amount of computation, efficient techniques for calculating the error function must be used. However, due to recent advances in computer hardware computational efficiency is not much of a problem. Another problem with this technique is that with a complicated multivariable weighting function, a number of local minima may be present. If difficulties arise in computing a suitable solution a number of optimization algo-

rithms may have to be combined into a more robust optimization routine. For example, a random optimizer could be used to jump out of local minimums. At present I have found that by picking initial conditions intelligently and by using a direct search optimization algorithm, suitable solutions can be obtained.

3.5 Optimization Technique

There are many different optimization techniques which have been used previously some of which are suited to large multivariable optimization problems. Random methods, gradient methods and direct search methods make up the majority of the techniques. In general, random optimization techniques are used where good initial conditions are not present to start with. It is usually employed in combination with other techniques such as the symplex method or method of steepest descent. The optimization technique used was a direct search method called the symplex method by Nelder and Mead [10,11]. It was found that this was a sufficient optimization routine for this design problem.

A general symplex is a set of (n+1) points in an n-dimensional space. For a regular symplex the points are mutually equidistant and for a general symplex the points can be irregularly spaced. The idea behind the algorithm is to eventually end up with the symplex around the minimum. This is accomplished by performing four different operations on the symplex. Expansion, contraction, reflection and shrinking. The amount that the symplex is expanded contracted or reflected by is user defined. By conducting a series of tests on the vertices, the desired operation is determined. Convergence occurs when the diameter of the symplex is less than a pre-specified value. The choice of the initial symplex size and location also effects the solution obtained. The actual symplex algorithm used was contained in the Pro-Matlab™ toolbox and more information can be obtained from the references [12].

3.6 Description of Algorithms

The implementation of the antenna synthesis algorithm was done in Matlab™. The algorithm has a number of stages which are described in flowchart form (Figure 3.11).

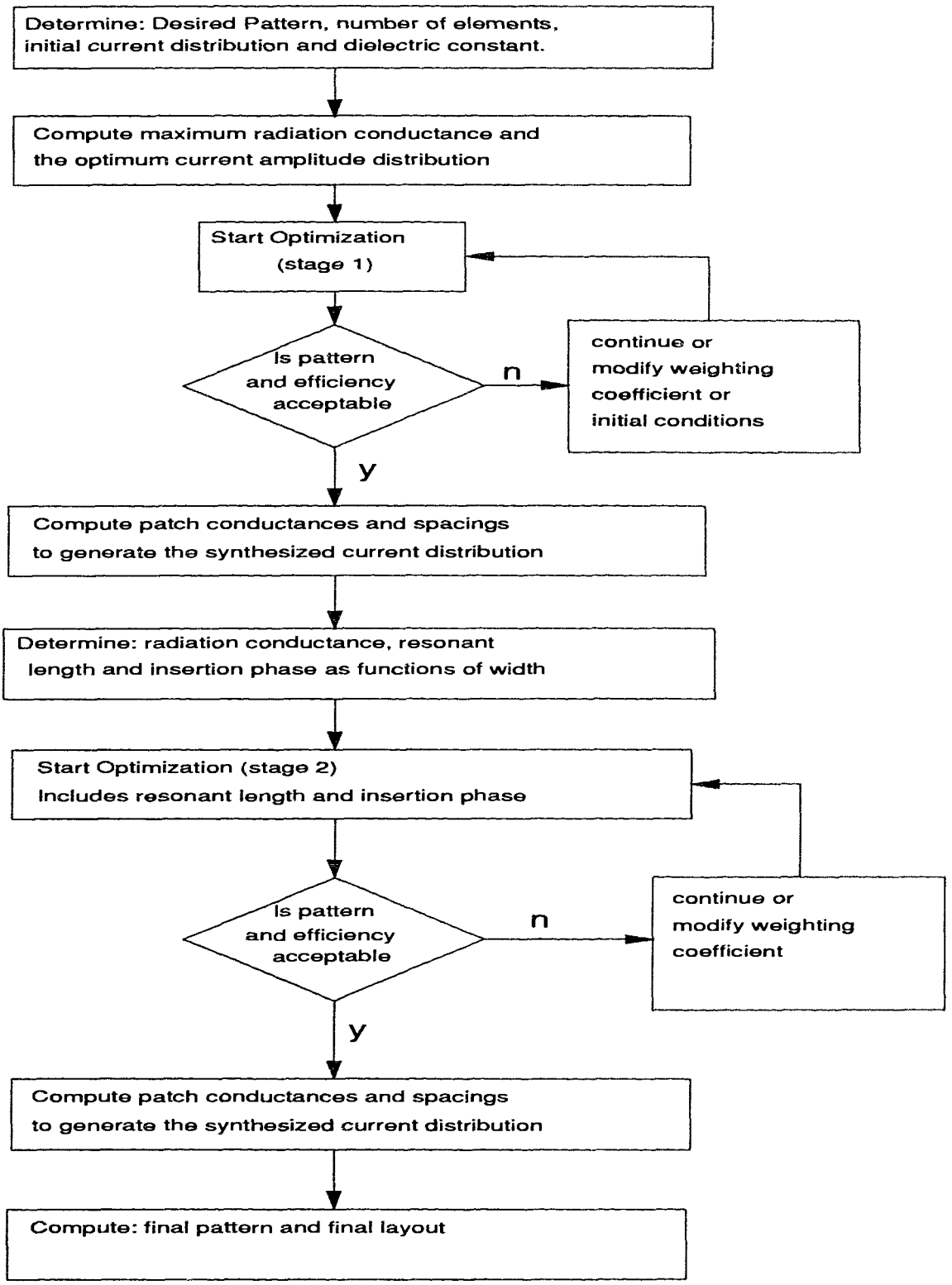

Figure 3.11 Design algorithm flowchart.

The first step in designing an antenna is to determine the desired pattern, the feedline impedance, and the dielectric constant of the substrate. Also determine the maximum patch width and the resulting radiation conductance. Use equation (3-31) to calculate the optimum current distribution. Finally, determine the initial conditions for the current distribution and start the optimization. If the optimization has difficulty proceeding then different initial conditions may have to be tried or the number of array elements increased. If necessary the optimization can be stopped at any time and the weighting function changed. When the results are satisfactory proceed to the next stage.

The next stage takes the desired current distribution computed by the first optimization routine and computes the radiation conductance and feedline length for each patch. First some approximate initial conditions are generated and then are varied until the desired current distribution is achieved. For example if the power radiated from a particular element is too low then the radiation conductance is increased. This procedure is repeated until the computed current distribution is equal to the desired current distribution. A similar procedure is used to compute the feed line lengths. The lengths are varied, one at a time, until the correct phase distribution is achieved. Since the amplitude distribution is slightly dependent on the phase distribution it may be necessary to run this procedure several times until the solution becomes stable.

The next thing to do is compute the resonant patch length, radiation conductance, and patch insertion phase as a function of patch widths. The most convenient way to determine the resonant patch lengths is to use Touchstone™. A table can be generated with the patch length, conductance and insertion phase as functions of patch width. Another optimization is then performed with varying patch lengths and insertion phase taken into account. Including these

two factors will cause some change in patch spacing. However, they have only a minor effect on the final solution. After the second optimization is completed the final solution is checked and the patch antenna layout file is generated.

Initial conditions for the optimization can take many forms. A method that works fairly well is to first set the magnitude of the current distribution to that of the optimum power efficient distribution. Then set a tapered phase distribution so that the beam is pointing in the direction of the desired main beam. Many modifications of these initial conditions can be tried some leading to different final solutions.

4 ANTENNA RANGE DESIGN AND CHARACTERISTICS

An antenna test range is a measurement setup designed to measure far-field radiation patterns, cross polarization, and gain, of an antenna. Through the utilization of a Hewlet Packard network analyzer (HP8510A), multipath effects which occur in a typical antenna test range could be time gated out of the measurement [14,15]. This reduces the need for a costly anechoic chamber and antenna tower which typical antenna ranges use [5,13]. Time domain gating is an effective way to eliminate multipath reflections from antenna measurements. However, some limitations are present and have to be considered when using this technique.

Multipath reflections occur when an electromagnetic wave reflects off the ground and/or nearby objects such as buildings. These reflections combine with the direct-path signal causing distortion in pattern measurements. Multipath effects can be reduced considerably using the time-domain gating feature of the HP8510. This is done by using the HP8510 to measure the swept frequency response of the antennas and then computing the Inverse-Fourier transform to give the time domain impulse response. Due to different path-lengths for reflected signals the time domain responses of these signals will occur later in time than the direct path signal. A gate, which is simply a time-domain filter, is then applied to suppress the unwanted reflections. Converting the gated signal back into the frequency-domain gives the direct path response with multipath effects suppressed.

Difficulties arise with gating when the antenna being measured has a narrow bandwidth. Since narrow bandwidth signals have spread impulse responses, it may be difficult to separate the direct-path impulse response from multipath responses. In some cases they overlap considerably. Subsequent sections will describe how to approximate the length of the impulse response of an antenna as well as methods to get around the bandwidth limitation of this technique.

4.1 Antenna Range Theory

Most of the far-field antenna ranges described in the literature [5,13,16] can be represented by the general model shown in Figure 4.1.

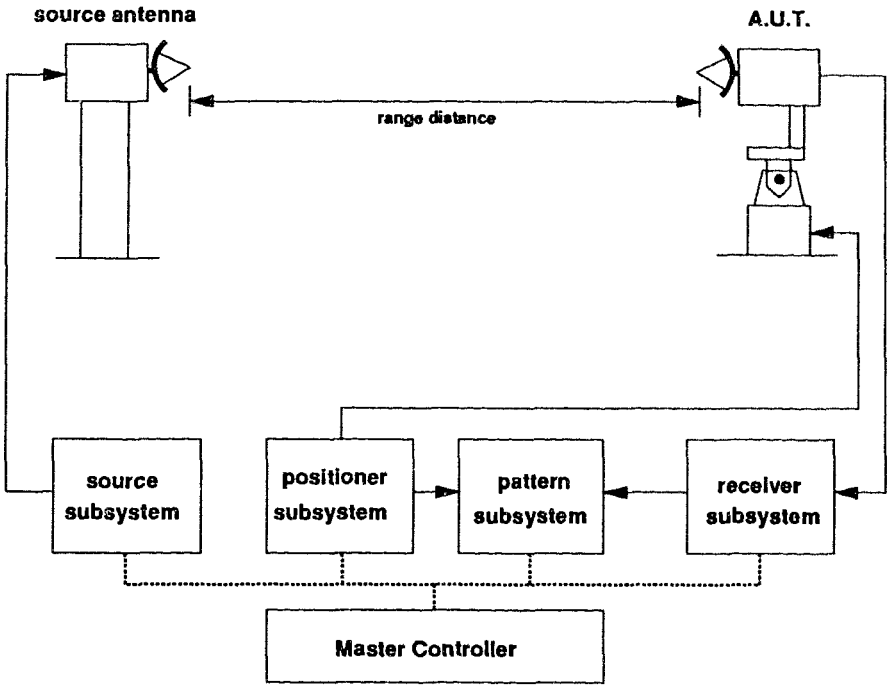

Figure 4.1 A general model of an antenna range.

The Receiver Subsystem must be capable of measuring amplitude and phase (optional) of the received signal from the antenna under test (AUT). Wide power level variations between peaks and nulls of a radiation pattern require the receiver to have a wide dynamic range and be linear over this range. The receiver must also have a broad bandwidth to accommodate a reasonably large frequency coverage. Sensitivity is also important to accurately measure low power signals at nulls in the pattern. Receiver sensitivity can be improved by using a low noise amplifier (LNA) to boost the received signal. By using the HP8510 the receiver also has the added advan-

tage of being able to use the source as a reference signal for phase-locking to the received signal. This brings about the advantage of better noise suppression as well as rejection of unwanted signals in and around the same frequency band.

The Source Subsystem is generally a frequency source which provides transmit power to the source antenna. High output power, broad frequency coverage and frequency stability are all desirable characteristics of the source subsystem. To perform Time-Domain-Gating the source should have a stepped-phase-locked output ability in order to obtain the most accurate measurements possible.

The Positioner Subsystem (Pedestal) moves the antenna to different angles in order to facilitate pattern measurements. Typically the pedestal should have two or more degrees of freedom in order to have sufficient measurement flexibility. For pattern measurements on most antenna ranges, azimuth over elevation axis [5] are the most suitable. Typically the elevation is set to a fixed value and azimuth is stepped through a number of angles.

The Pattern Recorder Subsystem records 2D graphs of radiation power as a function of azimuth or elevation angle. In modern systems a computer with a graphics card and an external printer can be used as a pattern recorder.

The Master Controller controls all of the subsystems in the antenna test range and is used to synchronize and organize various tasks which subsystems perform. The master controller is usually a microcomputer with various types of interface hardware attached. Measured data and parameters can also be stored on the system controller.

4.2 Far-Field Condition Calculations

In order to properly measure the characteristics of an antenna, care must be taken to ensure that the far-field condition is met. This condition is used to ensure that near-field radiation components have died out and only far-field components are being measured. A rule of thumb for determining the minimum required distance between the source antenna and AUT [5,13] for far field conditions is

$$d_{min} = \frac{2D^2}{\lambda}. \tag{4-1}$$

where D is the maximum dimension of the aperture of the largest antenna in the range and λ is the free space wavelength. Typically this distance is increased slightly to offer a safety margin. Values of the minimum range distance for an antenna with length equal to 5λ are shown in table 4.1.

Table 4.1 Minimum distance values D=5λ.

Frequency (GHz)	λ (m)	d_{min} (m)
0.8	0.375	18.8
1.0	0.300	14.0
4.0	0.075	3.8
8.0	0.0375	1.9
12.0	0.0250	1.3
18.0	0.0167	0.83

4.3 Antenna Range Block Diagrams

This section shows the design of the antenna measurement system. As stated, the system hardware and software are sufficiently flexible to allow for a wide range of measurement conditions.

When the specific conditions of the measurement have been determined the antenna measurement system can be tailored to the users needs. To accomplish this some calculations should first be performed to determine various measurement conditions and setup conditions. These Calculations will be presented here briefly.

A block diagram of the antenna range for pattern measurements between the frequencies of 800 MHz to 4 GHz is shown in Figure 4.2. Above 4 GHz a similar system can be used except the amplifiers have to be replaced with higher frequency amplifiers. Other system configurations are also possible using an HP8341B Frequency Synthesizer for the source subsystem and an HP8902A Measuring Receiver for the receiver subsystem. At present this equipment is in house, however, gating cannot be used with it.

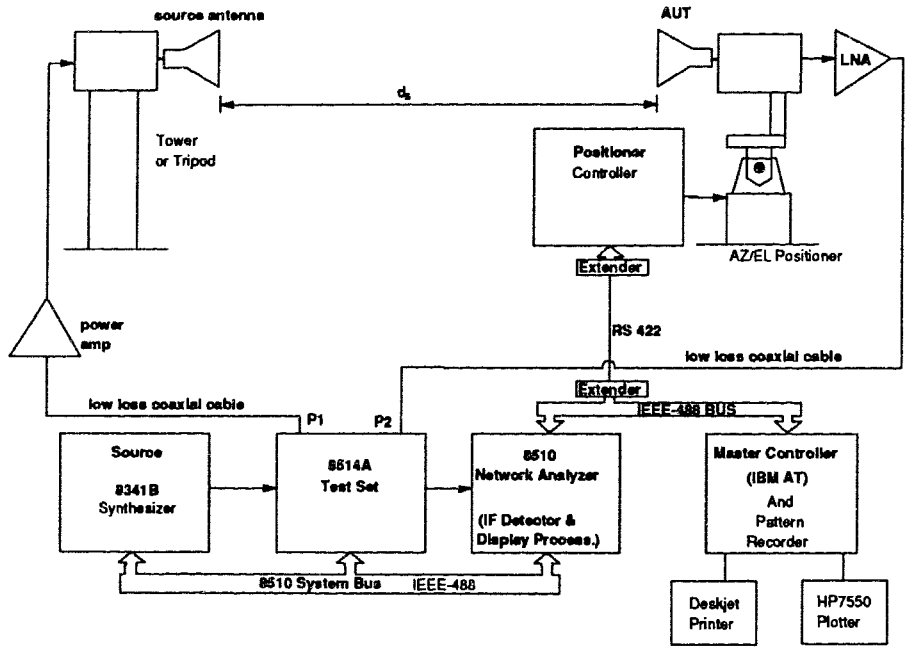

Figure 4.2 Block diagram of the antenna range.

4.3.1 HP8510 Network Analyzer

The source and the receiver subsystems for this antenna range are implemented using an HP8510A network analyzer equipped with an 8341B Synthesized Sweeper, an 8514A S-Parameter Test Set and the time domain option. The source and the test set are controlled by the HP8510 through the 8510 System Bus. By using the HP8510 to measure S_{21} the ratio of received to transmitted power is obtained. In order to increase the dynamic range of the system and to compensate for signal loss in the cables a power amplifier is used at the transmitting antenna and an LNA is used at the receiving antenna. Since the cabling and amplification in the system clearly offset S_{21}, the S_{21} measurement can be used as a relative measurement only. The data can be either normalized to obtain the antenna pattern or compared with that of a standard gain antenna.

4.3.2 Tripods and Pedestals

The source antenna is placed on a tripod, balcony or a roof top location in order to minimize the effect of its image in the ground plane. The AUT is mounted on the Azimuth over Elevation Antenna Pedestal by either bolting the AUT directly to the pedestal turn-table or by using a small standoff tower or plastic mast.

4.3.3 System Controller

The system controller is 386 personal computer operating in a DOS environment. Its essential features are a VGA graphics card and an IOTEK™ IEEE-488 card. The required software on the machine is the IOTEK™ IEEE-488 driver, Turbo Pascal™ 5.1, Graftool 3D 3.0 and the Antenna Measurement Program (AMP). An HP Deskjet plus printer and an HP7550A plotter are used as

hard copy devices. The system controller controls the HP8510A and the antenna pedestal. After the measurement is complete the system controller plots the data and stores it. Graftool can be used to obtain presentation quality plots of the measured data in many forms including polar plots and 3D polar plots. In any modifications need to be done on the AMP program it will be convenient to have Turbo Pascal loaded on the machine.

4.4 System Software

The system software for the antenna measurement system is an interactive software designed to command the various subsystems in the antenna range. At present the program is designed to interface to the HP8510 and the Daedal antenna pedestal. However, due to the programs modular design it can be easily upgraded or modified to control other measurement subsystems.

4.4.1 Main Menu

The main menu chooses the various main commands to be executed. The commands which the program performs are as follows:

(a) **Set Measurement Type.**

Sets the desired measurement type and allows the user to modify the measurement parameters. Measurement Types are as follows:

-Magnitude versus Azimuth (for up to 5 frequencies)
-Magnitude versus Azimuth (for up to 5 Elevations)
-Magnitude versus Azimuth (save phase data)
-Magnitude versus Elevation (for up to 5 frequencies)
-Magnitude versus Elevation (for up to 5 Azimuths)
-Magnitude versus Elevation (save phase data)

After selecting the measurement type the measurement parameters, such as start angles, stop angles, step angles and frequencies, can be modified. Parameters which are related to the HP8510 such as gating time, acquisition modes, calibration, etc. should be setup using the HP8510 front panel before the measurement is started.

(b) Set Plot Reference Value

Allows 0dB on the plot to be referenced to this value.

(c) Enter Pedestal Geometries

Allows for the entry of the antennas aperture position relative to the intersection point of the pedestals axis. This allows for the center of the gate to be moved during measurement in order to compensate for the movement of the test antenna aperture relative to the transmit antenna. As shown in Figure 4.3a, as the antenna is rotated the aperture moves further away from the transmit antenna. This results in a shifting of the time domain impulse response. If gating is used then the impulse response may no longer lie in the gate window. To compensate for this the gate window can be moved. The program uses simple geometry to calculate the shift in the gate window using the current pedestal angles as well as the user supplied pedestal geometries. The dimension *a* as indicated in Figure 4.3b is called the azimuth aperture rotation radius and the dimension *b* is called the elevation aperture rotation radius.

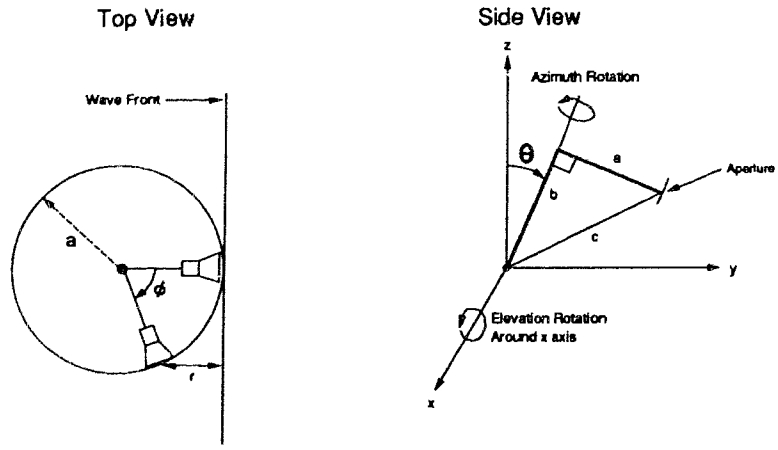

Figure 4.3 Explanation of dynamic gating.

(d) Standard Gain Calibration.

Allows the user to measure a standard gain antenna at bore site to be used as a reference for other measurements.

(e) Move Pedestal

Allows the user to move the pedestal to a desired position. The move can be accomplished using the cursor keys or by typing in the desired position. The home position can also be reset. This allows the user to boresight the antenna and then reset the home position to boresight.

(f) Save Setup

Saves Measurement Parameters and HP8510 setup parameters to files. The Measurement parameters are stored under "filename.PAR" and the HP8510 setup parameters are stored under "filename.HPS".

(g) Recall Setup

Recalls the previously saved setup.

(h) Start Measurement

Starts the measurement. At this time a polar graph is displayed showing points as they are measured. When the measurement is complete, the program will beep and wait until a key is pressed. The program can be halted at any time by pressing "ESC".

(i) Replot

Replot the data normalized with respect to the maximum or standard gain.

(j) Save Data

Save measured data in an ASCII file. Also save the measurement parameters in a separate file.

(k) Recall Data

Recalls already saved data in order to be displayed. This command overwrites data already stored in memory.

(l) Exit Program

4.5 Time Domain Gating Considerations

Most of the information necessary to understand how time domain gating works can be found in the HP8510 manuals [17] and other references [14,15]. By using time domain gating unwanted reflections can be removed from the desired measured signal. This is very advantageous since good pattern measurements can then be obtained without using an anechoic chamber. It should, however, be stressed that time domain gating cannot eliminate all reflections since some reflections have path lengths which are too close to that of the main signal path length. This problem

is more severe when measuring narrow-band antennas.

Software gating, as used in the HP8510, has some inherent limitations when used for antenna measurements. One of the main problems has to do with the width of the time domain impulse response for a particular antenna. This smearing of the impulse response of the antenna leads to difficulties in gating out reflected signals since the responses may overlap. When using software gating the bandwidth of the antenna plays a major role in determining the pulse width of the time domain response.

The impulse width is inversely proportional to the Frequency Span of the measurement. From the HP8510 manual [17] the impulse width using the gating in bandpass mode with a "normal" window yields an impulse width of

$$\text{Impulse Width} = \frac{2}{\text{Frequency Span}} \tag{4-3}$$

If this is multiplied by the speed of light (3.0E+08 m/s) then the physical distance that this impulse response occupies is obtained. Clearly any reflected signal path will have to be at least this distance longer than the main signal path in order to prevent interference. For a typical microstrip patch antenna with a bandwidth of 2% the physical path widths are:

$$\text{Impulse Width}(3.5\text{GHz}) = 8.6\text{m} \tag{4-4}$$

$$\text{Impulse Width}(0.8\text{GHz}) = 37.5\text{m}$$

Clearly time domain gating is not an effective way for measuring narrow band antennas at low frequencies and other techniques will have to be used. For a travelling wave antenna operating at 3.5GHz the bandwidths reach up to 8%. Therefore, the response width is only a few meters, indicating that time domain gating is useful for such an antenna. However, with arrays there is another problem which causes spreading of the time domain response.

A typical array has variable path lengths from each radiating element to the feed point (Figure 4.4). This implies that a number of impulses may be received for a given array, each impulse separated slightly in time. This causes further spreading out of the impulse response. The position of the elements relative to the incoming wave front also has an effect on this spreading out effect. For the antenna presented in this thesis, which is about 1 meter long, the spreading out effect is limited to a few meters at best. So the overall impulse width for the travelling wave microstrip patch antenna is at most 4 or 5 meters. Separating the source antenna and the antenna under test by a sufficient distance ensures that reflected signals can be gated out of the measurement.

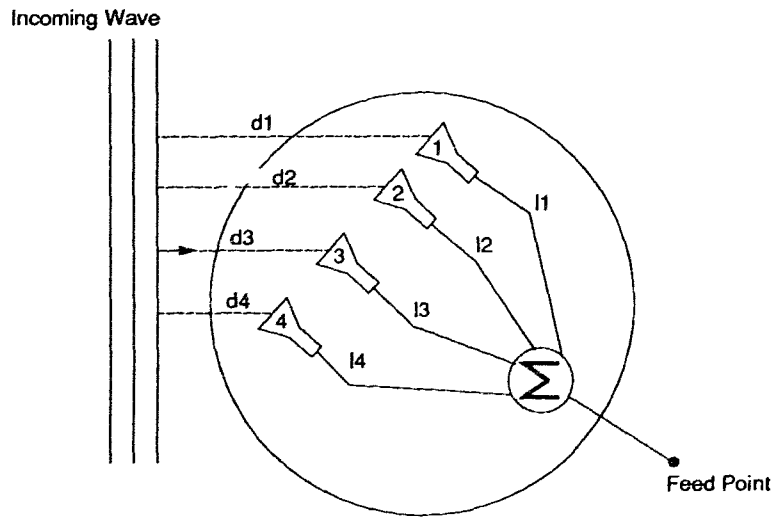

Figure 4.4 Different path lengths for impulses received by an array.

4.6 Range Site Selection Criterion

Since it is impractical to rely totally on gating for antenna measurements, some attention has to be paid to the site selection. When selecting a site the first criteria to meet is that of the far field condition stated in equation (4-1). In order to use time domain gating it may be necessary to

increase this distance in order to further separate the main and reflected signal paths. Keeping this in mind the site should also be free of signal cluttering objects such as rocks, trees, cars and buildings. Since most antennas are measured near the ground there will always be some reflection from the ground. By elevating the source antenna this reflection path length will be kept sufficiently longer than the main signal path as shown in Figure 4.5.

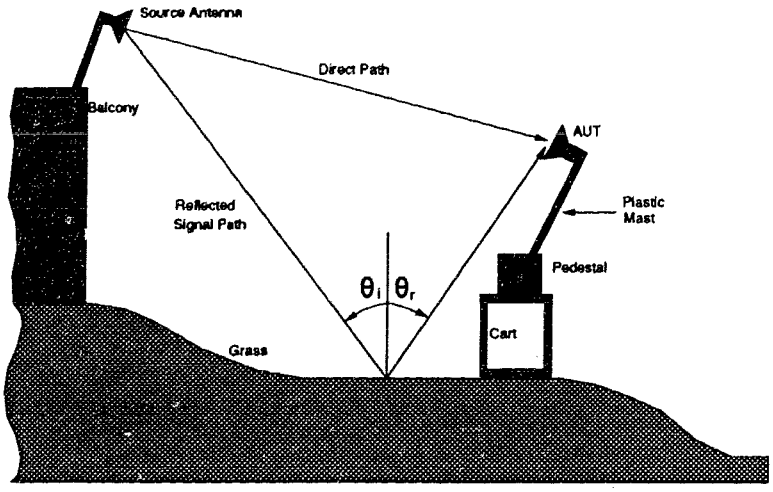

Figure 4.5 Antenna range site.

4.7 Range Specification and Verification

In order to verify the antenna range operation as well as the effectiveness of the time domain gating, some horn antennas were measured. The antenna used in this experiment was an AEL H-5001 standard gain horn antenna which works over the frequency range of 1GHz-2.5GHz. Measurements were done with gating on and these plots were compared to measurement plots supplied by AEL (Figures 4.6 to 4.13). In general these measurements agree extremely well indicating that the antenna measurement range works well.

The gated measurements were done with a gating window of 5.2ns which corresponds to 1.6 meters in free space. This dimension was derived by noting that each horn was about 0.5m long

and the bandwidth of the measurement was from 0.7-3GHz. Using equation (4-3) this corresponds to an impulse width of 1ns or 0.3 m. Since a small safety margin is needed the gating window was made slightly larger than the horns impulse response width of 0.5m+0.5m+0.3m=1.3m. It is wise to make the gating window as wide as possible to ensure that the desired antenna response is not gated out.

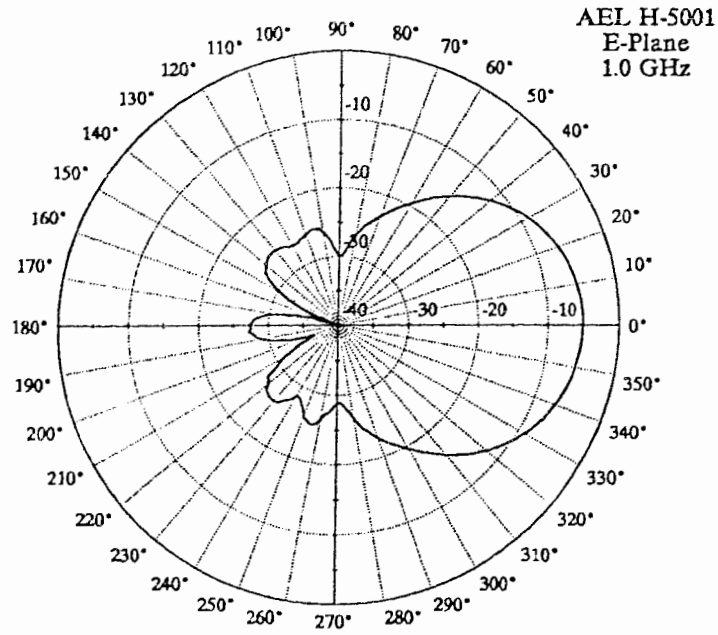

Figure 4.6 Measured Pattern

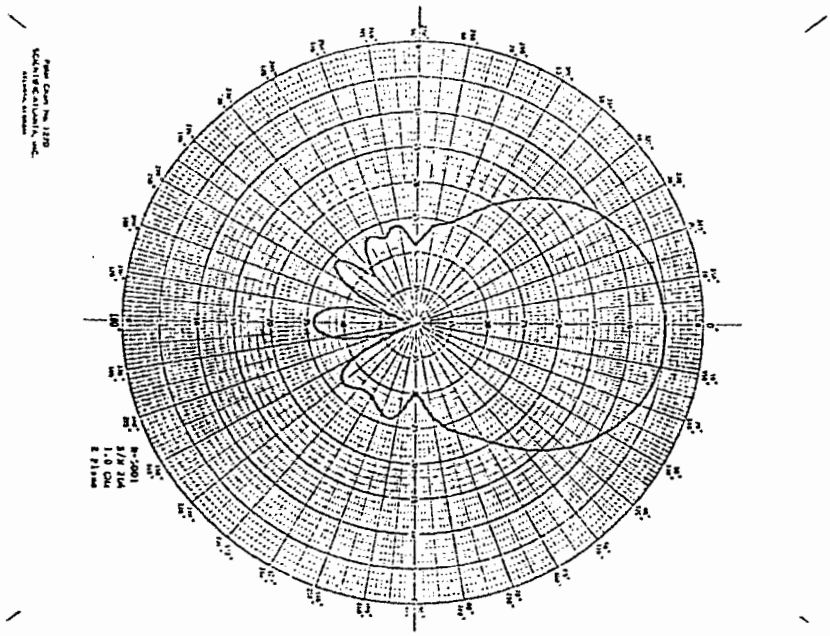

Figure 4.7 Pattern measured by AEL

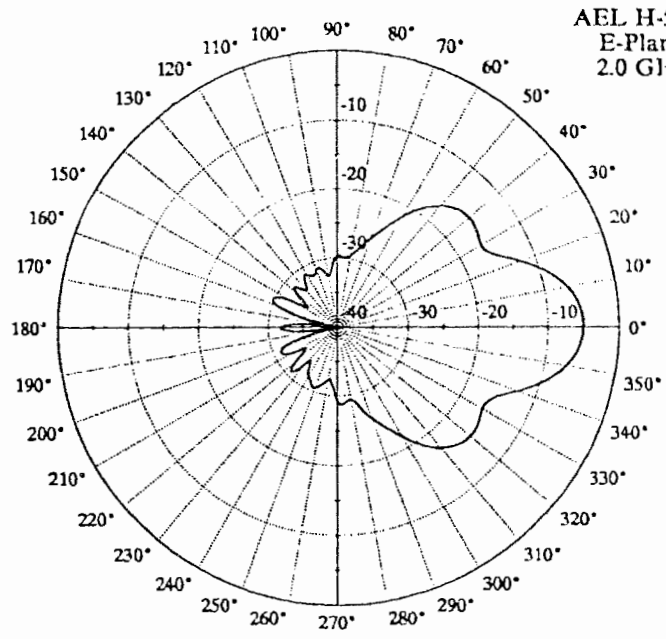

Figure 4.8 Measured Pattern

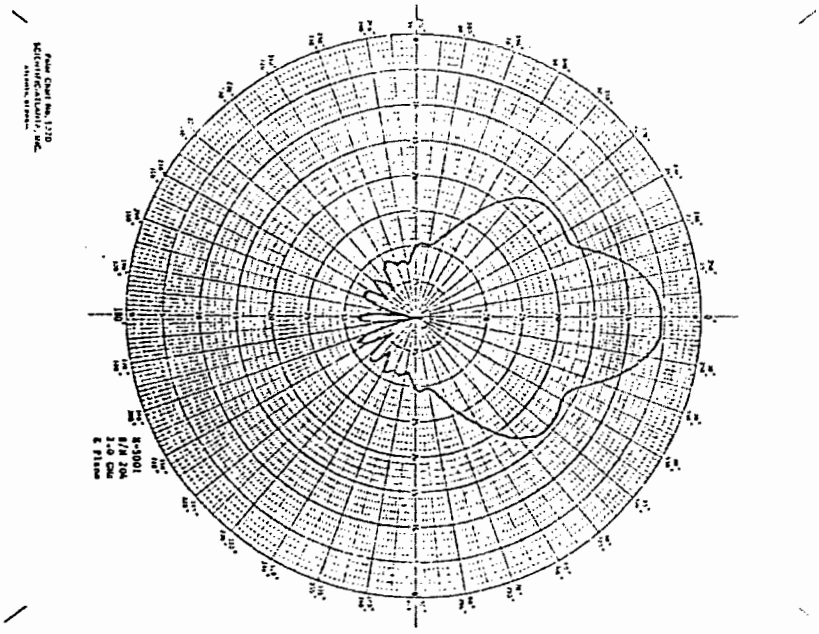

Figure 4.9 Pattern measured by AEL

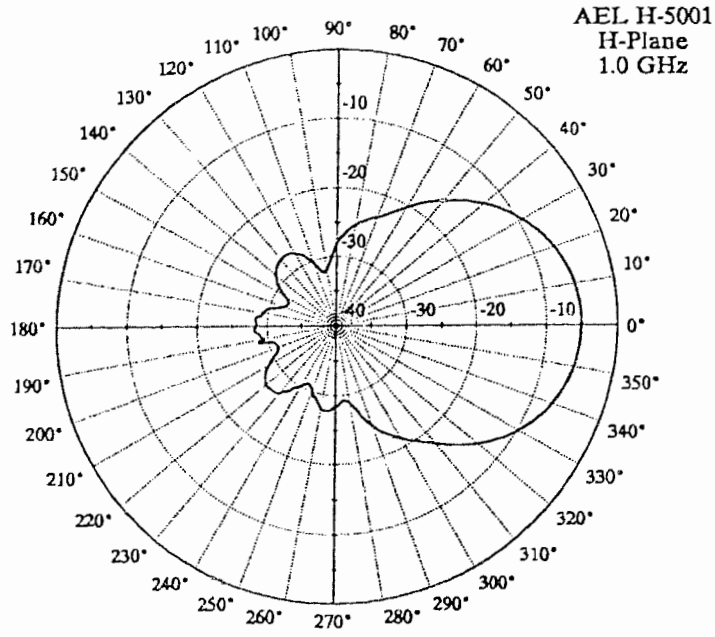

Figure 4.10 Measured Pattern

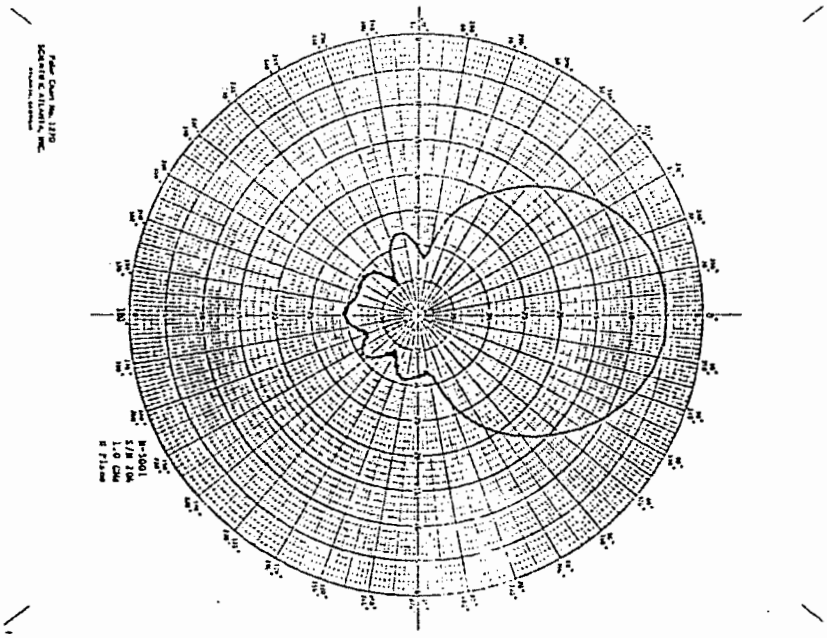

Figure 4.11 Pattern measured by AEL

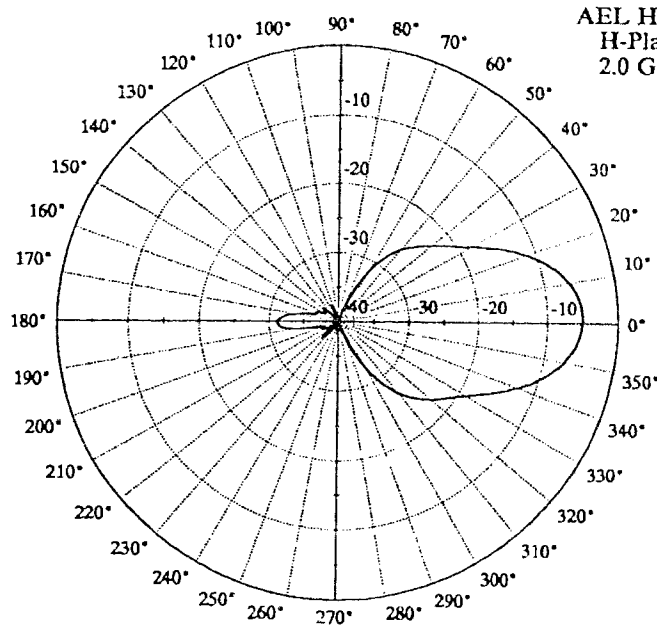

Figure 4.12 Measured Pattern

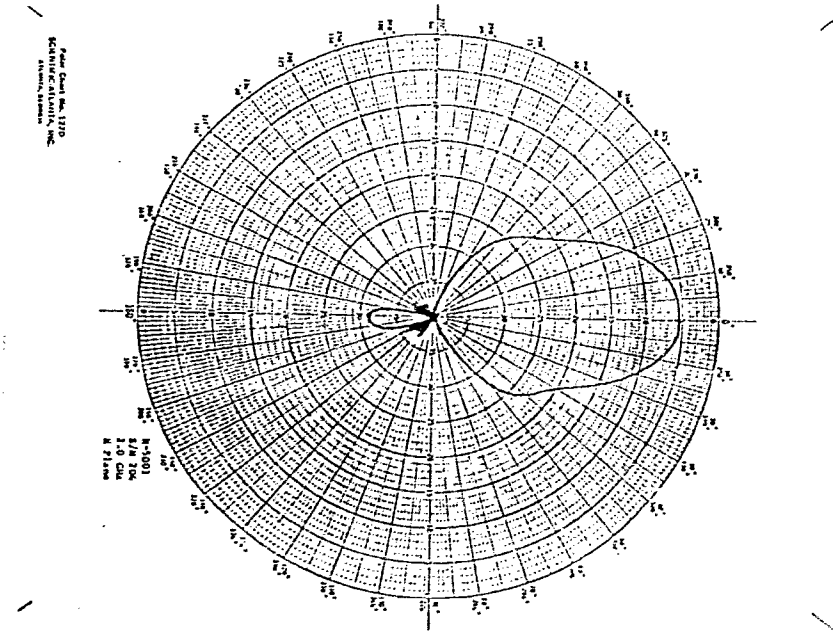

Figure 4.13 Pattern measured by AEL

Since the antennas designed for this thesis operate at 3.5GHz, a source antenna, which worked at these frequencies, was also needed. Some S-Band horns were found which had frequency spans from 2-4GHz. The patterns of these antennas were measured with the antenna range and are displayed in Figures 4.14 and 4.16. In order to demonstrate the effectiveness of the gating some pattern measurements without gating (Figures 4.15 and 4.17) were done. The patterns measured without gating show a higher level of pattern distortion, particularly for backlobes. This is due to the fact that reflections are low level signals that can only significantly distort other low level signals.

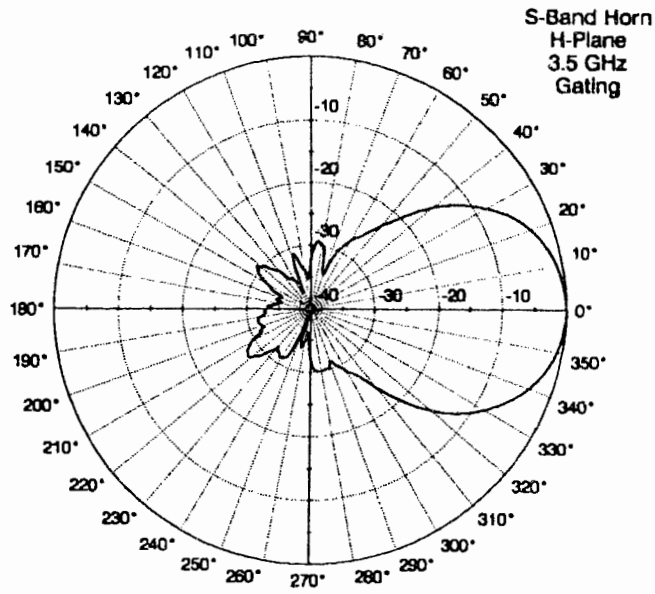

Figure 4.14 Pattern of S-band horn
(gating) (H-Plane) (3.5GHz)

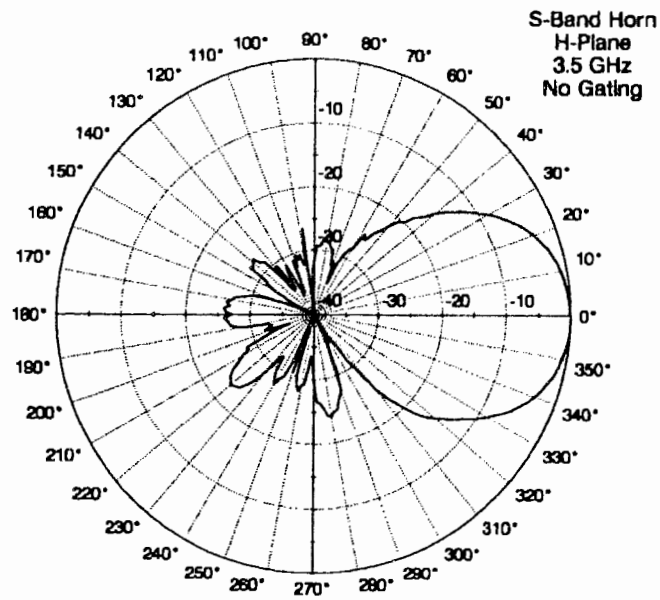

Figure 4.15 Pattern of S-band horn
(No gating) (H-Plane) (3.5GHz)

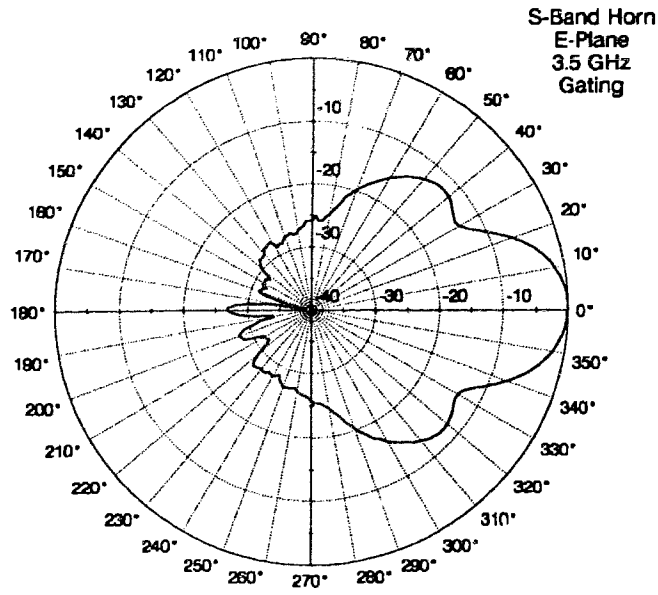

Figure 4.16 Pattern of S-band horn
(gating) (E-Plane) (3.5GHz)

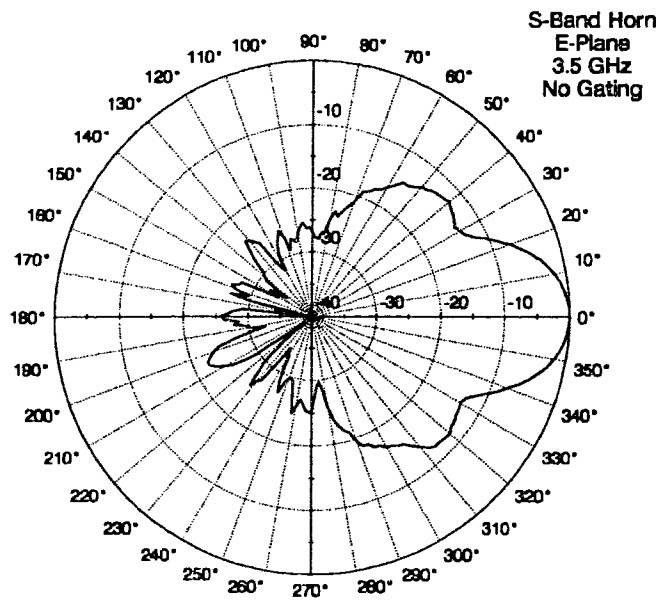

Figure 4.17 Pattern of S-band horn
(No gating) (E-Plane) (3.5GHz)

5 RESULTS AND DISCUSSION

In order to test the travelling wave patch synthesis algorithm presented in section 3, an antenna was built to synthesize a desired pattern. It was decided to keep the antenna size below one meter so that construction and testing would be kept as simple as possible. This meant that the design frequency had to be higher than the typical 800 MHz used in the mobile cellular band. Also the pattern beamwidth would have to be relatively large. In order to keep effects such as surface waves to a minimum, the substrate thickness was kept low. Some of the array design parameters were as follows.

Relative Dielectric Constant of Substrate	2.50
Substrate Thickness	30 mil
Center Frequency	3.5GHz

The desired pattern to be synthesized can be seen in Figure 5.1. The pattern was chosen somewhat arbitrarily, however, the shape is typical of that desired for an antenna on the rooftop of a building. Steeper inclination angles require increasingly less power since the mobile unit will be closer to the base station. Two different designs were completed for this pattern each stemming from different optimization weighting coefficients. The first antenna has an efficiency of around 74%, however, there is a significant error between the desired and designed antenna patterns. The second design has a pattern with low ripple. However, this is at the expense of a lower radiation power efficiency of 52%.

Figure 5.1 shows the desired and calculated antenna patterns for the first design.

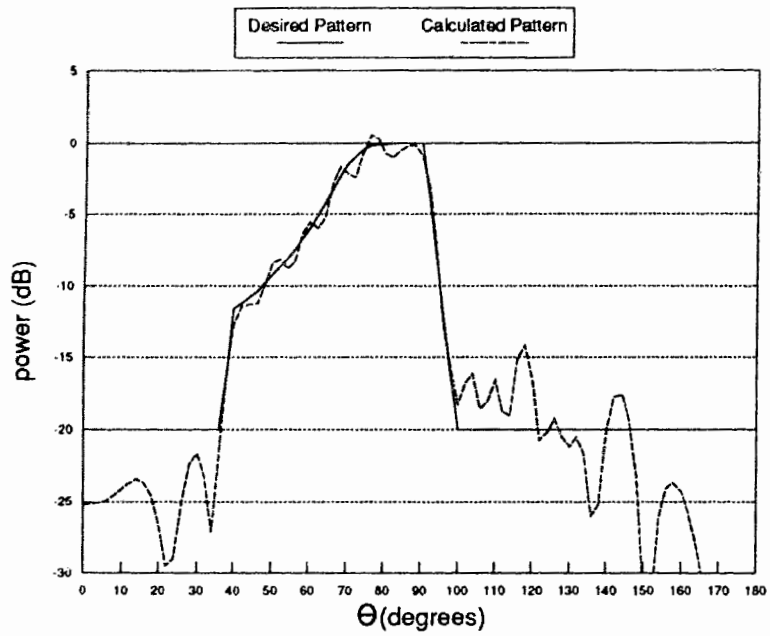

Figure 5.1 First design desired and calculated radiation patterns.

Figures 5.2 shows the current amplitude distribution of the antenna and 5.3 shows the phase distribution.

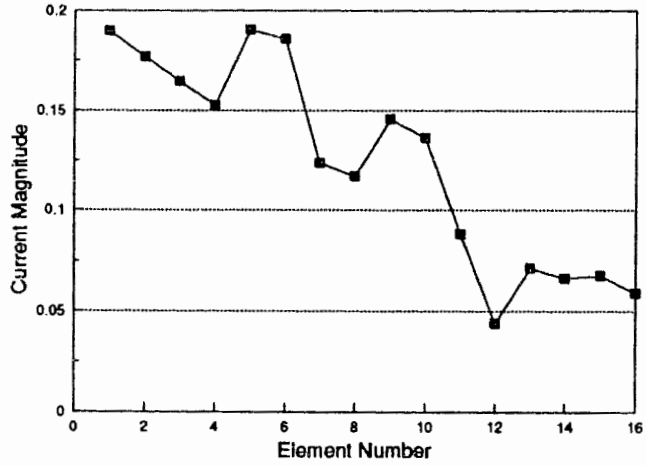

Figure 5.2 First design current amplitude distribution

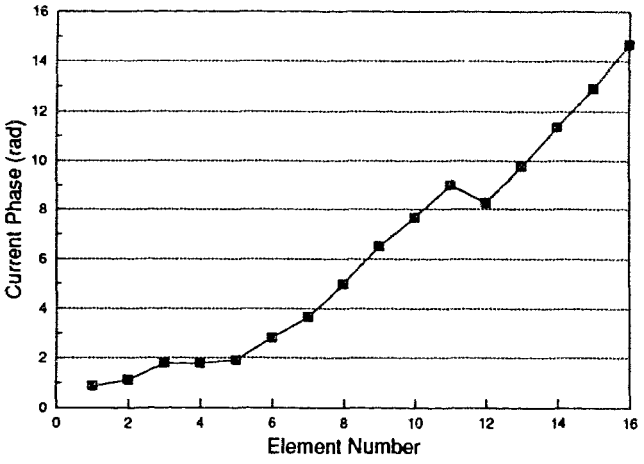

Figure 5.3 First design current phase distribution

The microstrip layout is shown in Figure 5.4. Note that in general all 16 patches are relatively wide which is a requirement of high radiation efficiency.

Figure 5.4 First design circuit board layout (5:1 scale).

Figure 5.5 shows calculated and measured patterns for the first antenna design. This graph indicates a fairly close correspondence between calculated and measured patterns. However, some discrepancies between calculated and measured patterns are present. These discrepancies are the result of several factors. After some analysis it was discovered that one of the main sources of error in the design is due to inaccuracies in the radiation conductance model. In particular the thinner patches radiate less than predicted. Another problem was introduced due to the fact that the antenna had to be manufactured in two pieces. The resulting microwave discontinuity at the

solder joint of the antenna results in a portion of power being reflected there. This reflection changes the current distribution of the antenna. The antenna pattern was slightly different every time the solder joint was modified.

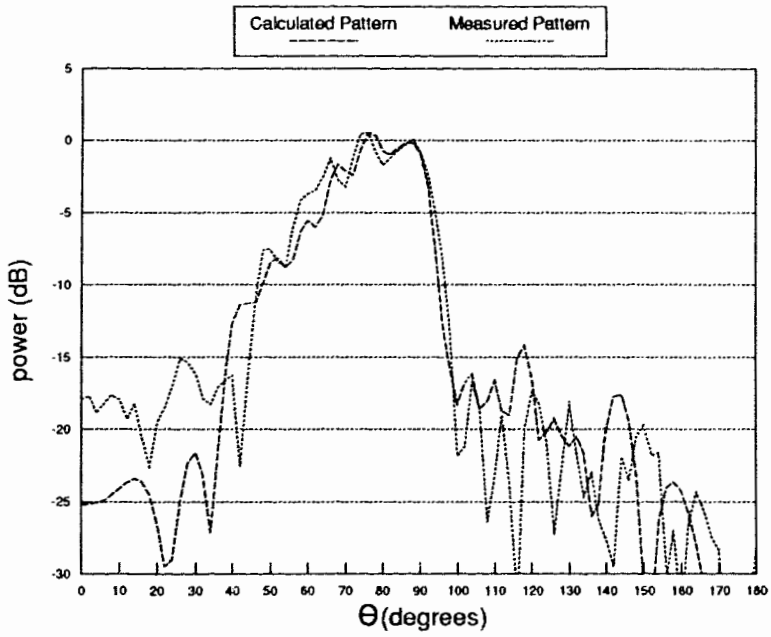

Figure 5.5 First design calculated and measured radiation patterns.

If the 2-port S-parameters of the antenna, between the feed and termination points, are measured then useful information about the antennas performance can be obtained. S_{11}, which is the input match, gives useful information about the VSWR bandwidth of the antenna. By measuring S_{21} the amount of power dissipated in the termination can be determined. This is a good check to see if the radiation conductances of the patches are correct. Figure 5.6 shows the measured S-Parameters of the first antenna design. The VSWR bandwidth of the antenna is around 7% for 10 dB return loss. S_{21}, however, is a better indicator of the useful bandwidth of this antenna since it represents the radiation efficiency and thus the antenna gain. S_{21} indicates a 7% gain bandwidth.

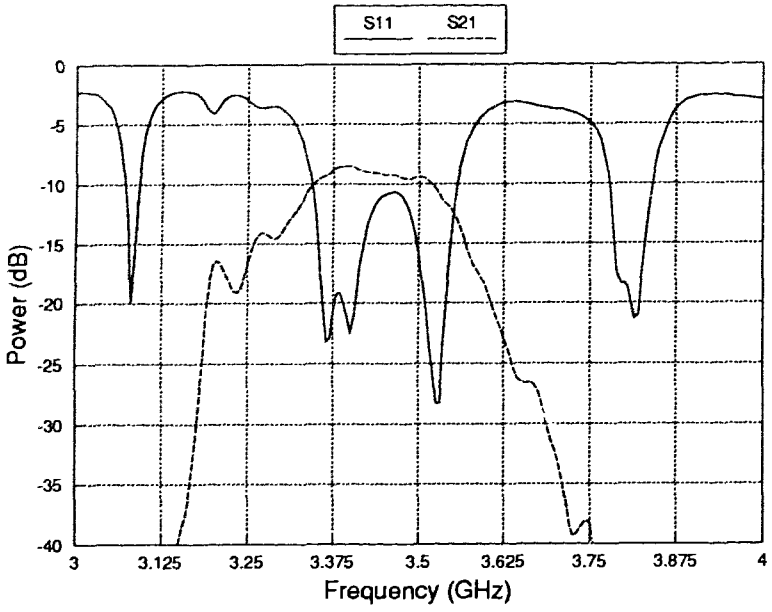

Figure 5.6 First design measured S-parameters.

Since variations in frequency will cause a change in the phase distribution, and thus the antenna pattern, it would seem that the limiting factor in antenna bandwidth may in fact be the pattern. In fact the pattern will shift as a function of frequency and the amount of shift which can be tolerated depends on the system the antenna is being used in. It may in fact be useful to include frequency performance of the pattern in the pattern synthesis algorithm.

Table 5.1 displays a summary of the first antennas specifications.

Table 5.1 Parameters of first array design

Number of Patches	16
Overall array length	0.78m
Frequency	3.5 GHz
Radiation efficiency	73.4%
Power dissipated in microstrip	14.5%
Power dissipated in termination (calculated)	12.1%
Power dissipated in termination (measured)	12%
Input Return Loss (calculated)	19 dB
Input Return Loss (measured)	16 dB
VSWR bandwidth (10dB return loss)	0.250 GHz (7%)

The second antenna was designed to obtain a better pattern fit at the cost of lower power efficiency. Figure 5.7 does indicate that this pattern is somewhat smoother than the first design's pattern.

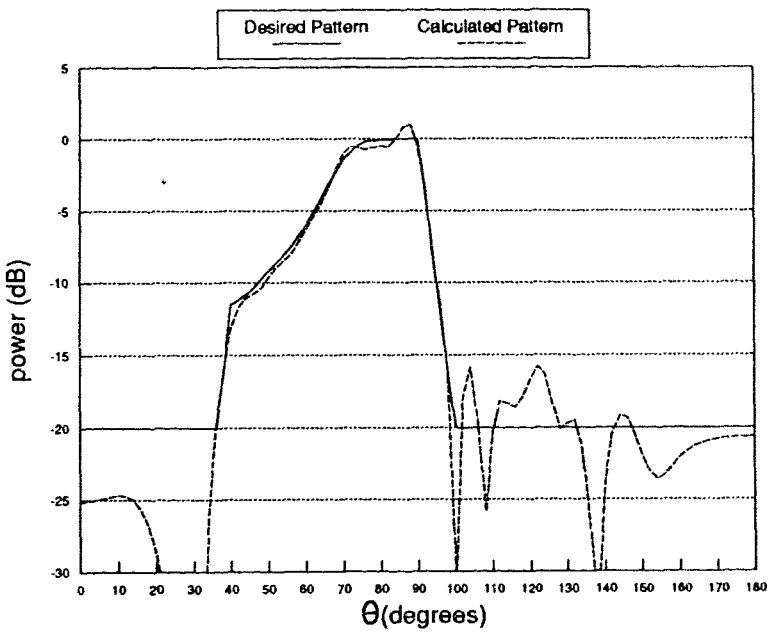

Figure 5.7 Second design desired and calculated radiation patterns.

Figure 5.8 and 5.9 show the amplitude and phase distributions of the second antenna design. Note that the amplitude distribution is more peaked than that of the first design. The amplitude distribution does not resemble the shape of the optimum efficiency current distribution given in Figure 3.6. As a result, this antenna design is only around 52% efficient. Figure 5.10 shows the layout for this antenna and Figure 5.11 shows the S-parameters.

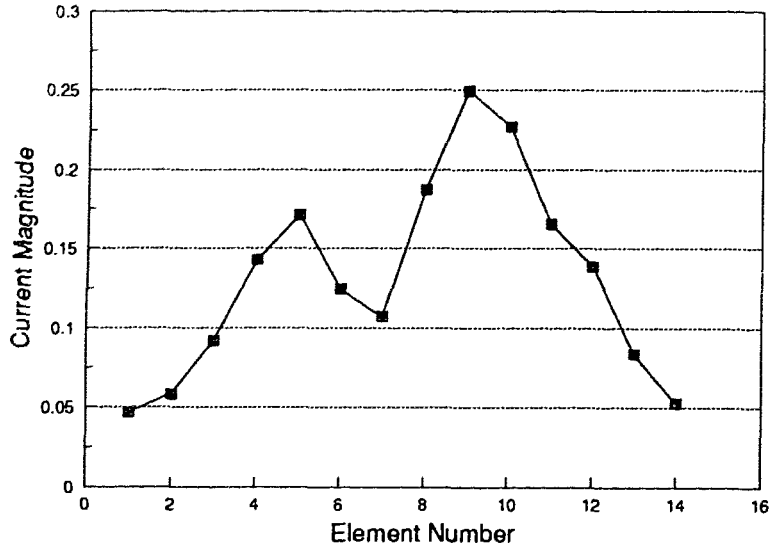

Figure 5.8 Second design current amplitude distribution.

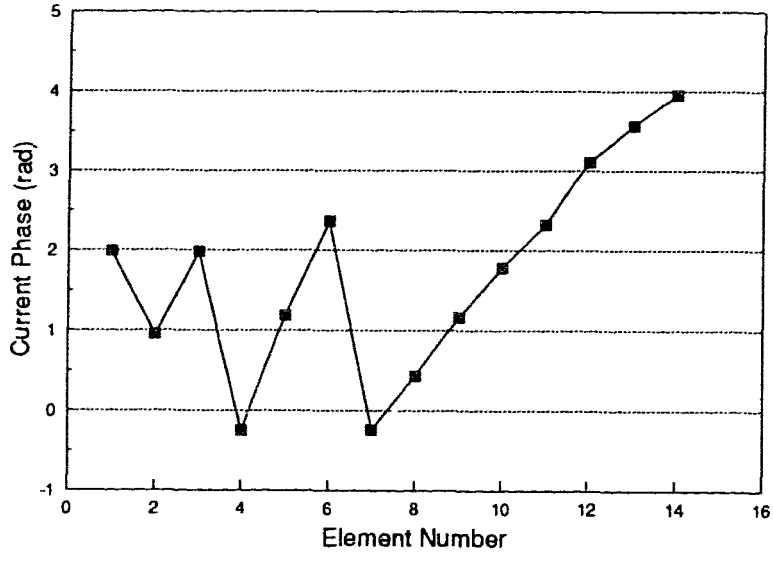

Figure 5.9 Second design current phase distribution.

Figure 5.10 Second design circuit board layout (5:1 scale).

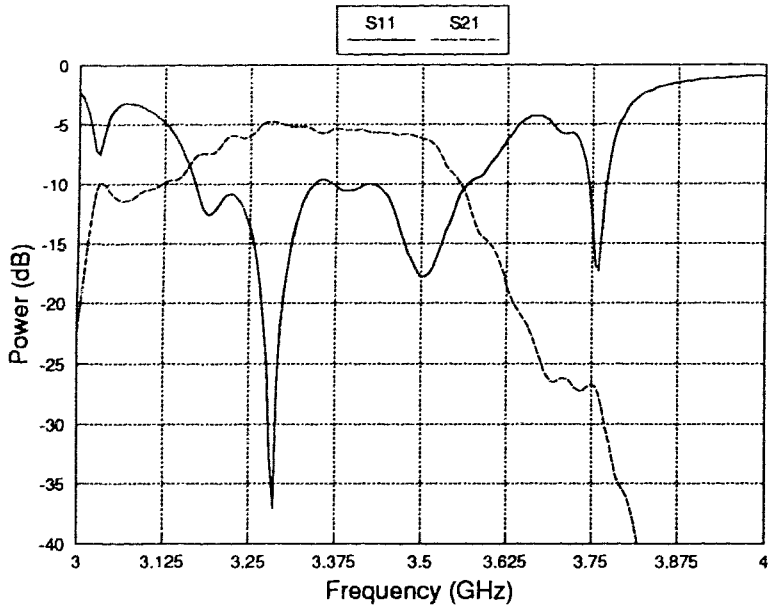

Figure 5.11 Second design measured S-parameters.

Figure 5.12 shows the second design's measured pattern. The null in the pattern was later found out to be due to inaccuracies in the radiation conductance model of the patches. After comparing the calculated and measured values of S_{21} it seemed that some of the radiation conductances in the antenna were too small. Since the first antenna, with the large patches, worked well it was decided that the narrow patches, in the second design, had radiation conductances which were too small. This hypothesis was verified by putting the measured pattern back in to the optimizer and allowing the radiation conductances to vary until the measured pattern was produced. Figure 5.13 shows the re-calculated pattern which is very close to the measured pattern. The current distribution resulting from the re-simulation verified this hypothesis that the radiation conductance of patches less than about 2cm in width, is lower than predicted. It was surmised that the reason for this is the effect of the microstrip feedline on fields at the patch ends.

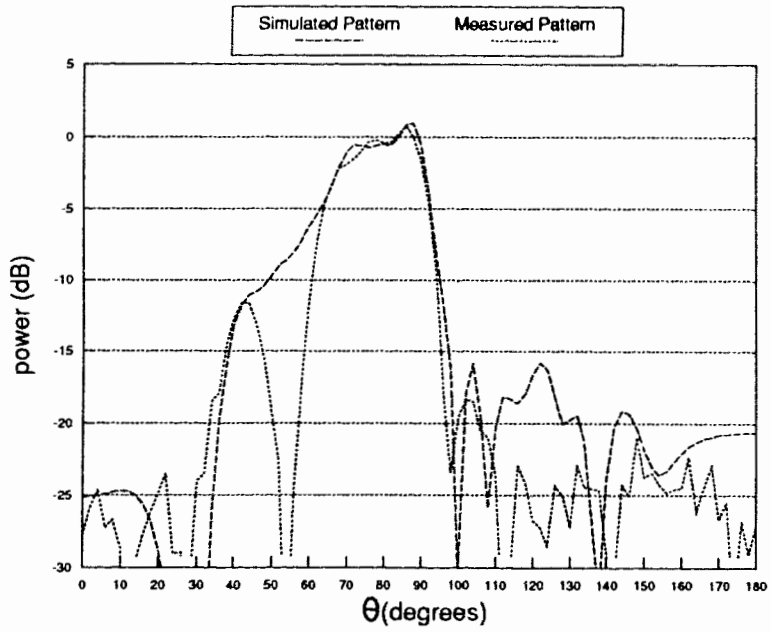

Figure 5.12 Second design calculated and measured patterns.

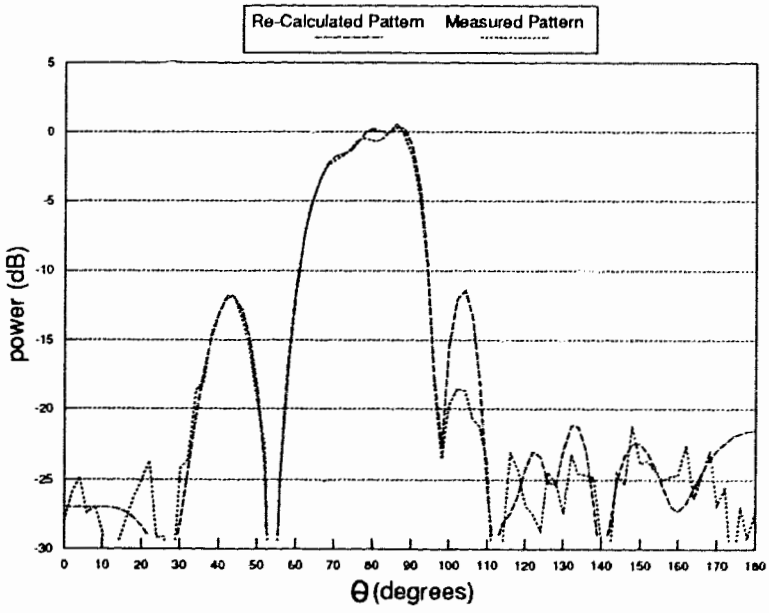

Figure 5.13 Second design re-calculated and measured patterns.

The measured pattern fit shown in Figure 5.12 indicates that a pattern fit which is better than in the first design was obtained. The measured pattern is quite smooth and closely follows the desired pattern in regions outside the null area. This good pattern fit was obtained at the cost of a lower power efficiency of 52%.

A summary of the antenna parameters is shown in table 5.2.

Table 5.2 Parameters of second array design

Number of Patches	14
Overall array length	0.78m
Frequency	3.5 GHz
Radiation efficiency	51.8%
Power dissipated in microstrip	21.4%
Power dissipated in termination (calculated)	26.8%
Power dissipated in termination (measured)	25.7%
Input Return Loss (calculated)	23 dB
Input Return Loss (measured)	17dB
VSWR bandwidth (10dB return loss)	0.375 GHz (11%)

6 CONCLUSIONS

The second chapter of this thesis offers some insight into the different pattern shapes achievable by using cylindrical antenna arrays. Varying the cylinder radius, the number of elements and the current distribution to these elements, varies the pattern beamwidth. Introducing a switching network adds 360° azimuth scanning capabilities. The beamwidth of the antenna can be dynamically controlled by varying the phase distribution to the elements, allowing for adaptable cell size.

Overall, the pattern synthesis algorithm for the travelling wave antenna worked quite well except for a few discrepancies in the radiation conductance model. The calculated and measured results clearly indicate that the algorithm is quite effective. Power efficiencies of 73% were achieved which are a substantial improvement of the 22% power efficiency obtained using Woodward's pattern synthesis method. The algorithm was found to be especially useful from an engineering point of view since tradeoffs inherent in all designs could be easily weighed against one another.

The antenna range functioned very well. Accurate patterns could be obtained without the use of an anechoic chamber as was indicated by the comparison of the measured patterns to that of AEL's. This antenna range was proven to be a cost effective alternative to large expensive antenna ranges.

Future recommendations for work on the mobile base station antenna include the design of economically feasible feed networks and further analysis of the advantages obtained by using this antenna in a communications system. Work which could be done on the pattern synthesis algorithm includes modelling or measuring the radiation conductance of the narrow patches. For the antenna range it would be useful to enhance the antenna range program to include useful features like direct pattern print out.

7 REFERENCES

[1] Jerry E. Boyns et-al, "Step-Scanned Circular-Array Antenna," *IEEE Trans. Antennas and Propagat*, Vol. AP-18, No. 5, pp. 590-596, Sept. 1970.

[2] Alan E. Holley, Edward C. DuFort and Robert A. Dell-Imagine, "An Electronically Scanned Beacon Antenna," *IEEE Trans. Antennas and Propagat*, Vol. AP-22, No. 1, pp. 3-12, Jan. 1974.

[3] A.G. Derneryd, "Linearly Polarized Microstrip Antennas," *IEEE Trans. Antennas and Propagat*, Vol. AP-24, No. 6, pp. 846-851, Nov. 1976.

[4] JR James and PS Hall, *Microstrip Antennas*, Volume 1, Chapter 10, IEE Electromagnetic Wave Series 28, London:Peter Peregrinus, 1989.

[5] Constantie A.Balanis, *Antenna Theory*, New York:Harper & Row, 1982

[6] JR James and PS Hall, *Microstrip Antennas*, Volume 1 and 2, IEE Electromagnetic Wave Series 28, London:Peter Peregrinus, 1989.

[7] Bevan B. Jones, Francis Y. M. Chow and Anthony W. Seeto, "The Synthesis of Shaped Patterns with Series-Fed Microstrip Patch Arrays," *IEEE Trans. Antennas and Propagat*, Vol. AP-30, No. 6, pp. 1206-1212, Nov. 1982.

[8] Y. T. Lo, D. Solomon and W.F. Richards, "Theory and Experiment on Microstrip Antennas," *IEEE Trans. Antennas and Propagat*, Vol. AP-27, No. 2, pp. 137-145, Mar. 1979.

[9] Guillermo Gonzalez, *Microwave Transistor Amplifiers Analysis and Design*, Englewood Cliffs, New Jersey.:Prentice-Hall, 1984.

[10] S.L.S. Jacoby, J.S. Kowalik and J.T. Pizzo, *Iterative Methods for Nonlinear Optimization Problems*, Englewood Cliffs, New Jersey.:Prentice-Hall, 1972.

[11] Brian D. Bunday, *Basic Optimization Methods*, London.:Edward Arnold Ltd, 1984.

[12] MathWorks Inc, *Pro-Matlab User's Guide*, South Natick, MA.:Mathworks, 1990.

[13] J. S. Hollis and Roland Moseley, "Siting Considerations in Microwave Antenna Measurements," *Scientific-Atlanta Inc.*, Aug 1961.

[14] John W. Boyles, "Measuring a Dipole Antenna Radiation Pattern Using Time Domain and Gating," *RF Design*, pp 44-49, Sept. 1985.

[15] Doren W.Hess, "Time-Gating of Antenna Measurements," *Scientific-Atlanta Inc.*

[16] "Antenna Measurements: Manual Pattern Measurements Using the HP 8510B," *Hewlett-Packard Application Note 374-1*, page 3

[17] Hewlet Packard,"HP 8510B Operating and Programming Manual," pp 1-15 (Time Domain Measurements), (1987).

[18] *Postioning Systems and Components 1990-1991 Catalog*, Daedal Positioning Tables & Controls, pp 148-151

[19] *Basic Antenna Measurements*, Scientific-Atlanta Inc., page 5.